THE USE OF TETRACYANOZINCATE(II) IN THE PREPARATION OF SUPRAMOLECULAR COORDINATION POLYMERS

by

Liang Ouyang
B. Sc., Peking University, 2003

THESIS SUBMITTED IN PARTIAL FULFILLMENT OF
THE REQUIREMENTS FOR THE DEGREE OF

MASTER OF SCIENCE

In the Department
of
Chemistry

SIMON FRASER UNIVERSITY

Spring 2007

APPROVAL

Name: Liang Ouyang

Degree: Master of Science

Title of Thesis: The Use Of Tetracyanozincate(II) In The Preparation Of Supramolecular Coordination Polymers

Examining Committee:

Dr. George R. Agnes
Chair
Professor, Department of Chemistry

Dr. Daniel B. Leznoff
Senior Supervisor
Associate Professor, Department of Chemistry

Dr. Vance E. Williams
Supervisor
Assistant Professor, Department of Chemistry

Dr. Jason A. Clyburne
Supervisor
Adjunct Professor, Department of Chemistry

Dr. Hua-Zhong Yu
Internal Examiner
Associate Professor, Department of Chemistry

Date Approved: December 19, 2006

ABSTRACT

Several coordination polymers using $K_2[Zn(CN)_4]$ as starting material have been prepared. $[Zn(CN)_4]^{2-}$ acts as a building block and source of free cyanide due to lability. A Cu(I)/Cu(II)/Zn(II) mixed-valent $[Cu(en)_2][Zn(NC)_4(CuCN)_2]$ polymer (en= ethylenediamine), which has a 2-D layer structure with six structurally inequivalent cyanides in four bonding modes, was characterized. By using mixed chlorinated solvent/aquous layers, complexes with solvent molecules incorporated were afforded: $[Cu(en)_2]_{0.5}[CuZn(NC)_4][C_6H_5Cl]_n$ and $[Cu(en)_2]_{0.5}[CuZn(NC)_4](CHCl_3)$. Both structures contain a 3-D diamonded array. Due to thermal motion and disorder of solvent molecules, further details were not clearly identified.

Three anhydrous microporous cyanometallate complexes and their non-porous hydrates were prepared: $KCoFe(CN)_6$ and $KZnFe(CN)_6$ with Prussian Blue type structure and $CoZn(CN)_4$. All three anhydrous complexes exhibit hydrogen affinity at cryogenic conditions. Their H_2 and N_2 adsorption isotherms are analyzed using different adsorption models, showing surface areas and adsorption capacities ranging from 399 to 615 m^2/g, and 0.77 to 1.01 wt% at 77K/1atm respectively.

Keywords: Tetracyanozincate; Prussian Blue; Gas Adsorption; Hydrogen; Coordination Polymers.

ACKNOWLEDGEMENTS

It is difficult to overstate my gratitude to my supervisor Prof. Danny Leznoff. Throughout my thesis-writing period, he provided encouragement, sound advice, good teaching, good company, and lots of good ideas. I would have been lost without him.

To my fellow group members: thank you for your friendship, suggestions and support. I would like to especially thank Michael Katz, for all the help he has given me to almost every aspect of my research over these past few years. Thank you to Alex Au who has worked with me as a Chem 481 student. Your hard work was greatly appreciated.

I would also like to express my gratitude to Dr. Fred Einstein and Dr. Ray Batchelor for helping me with solving and refining crystal structures. Mr. Miki K. Yang is also gratefully acknowledged for completing all the C, H, N analyses, as well as Dr. Ian Gay for teaching me about porosity measurement with the instrument which is designed and constructed by himself. .

And special thanks to my parents, Song Ouyang and Huimin Chen, especially my dear mother, for asking everyday when my thesis would be done. And thanks too to my girlfriend and soul mate Leona Liu Ou, I could not have completed my program without your support and encouragement.

The generous financial support from Simon Fraser University is also gratefully acknowledged.

TABLE OF CONTENTS

LIST OF FIGURES

LIST OF TABLES

LIST OF ABBREVIATIONS

Å	Angstrom
Anal	analysis
atm	atmosphere pressure
au	atomic unit
bipy	2,2'-bipyridine
br	broad
C	Celsius
calcd	calculated
cm	centimeter
deg	degree(s)
dien	diethylenetriamine
EA	elemental analysis
en	ethylenediamine
equiv	equivalent(s)
HS	high spin
IR	infrared
K	Kelvin

kJ	kilojoule
L	ligand
m	medium
MAS	Magic Angle Spinning
mg	milligram
mL	milliliter
mmol	millimole
mol	mole
M	metal
Me	methyl (CH_3)
n	number of moles
N_A	Avogadro's number
phen	1,10-phenanthroline
PXRD	Powder X-ray Diffraction
s	strong
SQUID	superconducting quantum interference device
Tc	critical temperature
TM	transition metal
tren	tris(2-aminoethyl)amine

vs	very strong
vw	very weak
w	weak
wt%	weight percentage
1-D	one dimensional
2-D	two dimensional
3-D	three dimensional
ν	frequency
°	degree
μ_{eff}	effective magnetic moment
μ_B	Bohr magneton.

CHAPTER 1: INTRODUCTION

1.1 SUPRAMOLECULAR CHEMISTRY

1.1.1 Introduction to Supramolecular Chemistry

In the past decade, supramolecular chemistry has become one of the fastest growing areas of experimental chemistry due to its ability to construct infinite two- and three-dimensional structures that may possess interesting catalytic, electronic, spectroscopic or magnetic properties or defined pores.[1] In general, all supramolecular compounds involve the self-assembly of building blocks via non-covalent interactions such as hydrogen bonding, metal-ligand coordinate bonds or van der Waals forces.[2]

The primary focus of this thesis is supramolecular coordination chemistry, which utilizes the strong coordinate bonds between metal centres and deliberately designed organic ligands to assemble multidimensional systems. Supramolecular coordination polymers have a number of attractive features. First, there is a diversity of metal coordination geometries that can be used as building blocks to control the building up of a wider range of structures. Moreover, the different electronic, magnetic and spectroscopic properties of a wide selection of transition metal centres can offer attractive possibilities for designing functional materials with tunable properties.

In order to achieve a desired structure, ligands and metal centres with specific bonding preferences and geometries should be deliberately selected. It is reasonable to hope that the reaction occurs as designed and the resulting self-assembly yields the intended structure. However, it's very possible that the reaction occurs in an unexpected fashion which sometimes can afford a result even more instructive and interesting than the intended one. In this thesis, I choose to accept those occurrences during all my experiments not as failure but rather as a gentle assistance by nature.

1.1.2 Transition Metal Cyanide Complexes

The use of anionic transition metal cyanide building blocks in supramolecular coordination chemistry dates back to 1704 with the discovery of Prussian Blue.[3] It is not only the earliest synthesis of a coordination compound recorded in history but also the first coordination polymer supramolecular structure. Since there are already a large number of reviews on cyanometallates, this section will only address the points that are related to the research of this thesis.[3,4]

Cyanometallates of transition metals generally are very stable, and quite soluble in polar solvents. Both the carbon and the nitrogen ends of cyanide can act as Lewis bases and coordinate to metal cation centres. Different types of cyano group binding modes are depicted in Figure 1-1. The bridging mode of Figure 1-1(b) is the most commonly observed type. The cyano groups of the coordination polymers described in this thesis show type (a) Terminal **C**-bound, (b) (Linear) μ_2-bridging, (d) μ_2-C-bridging and (f) μ_3-bridging in their structure.[3]

The infrared spectrum is a very important tool for the determination of cyanide's binding modes and will be discussed in a later part of this chapter.

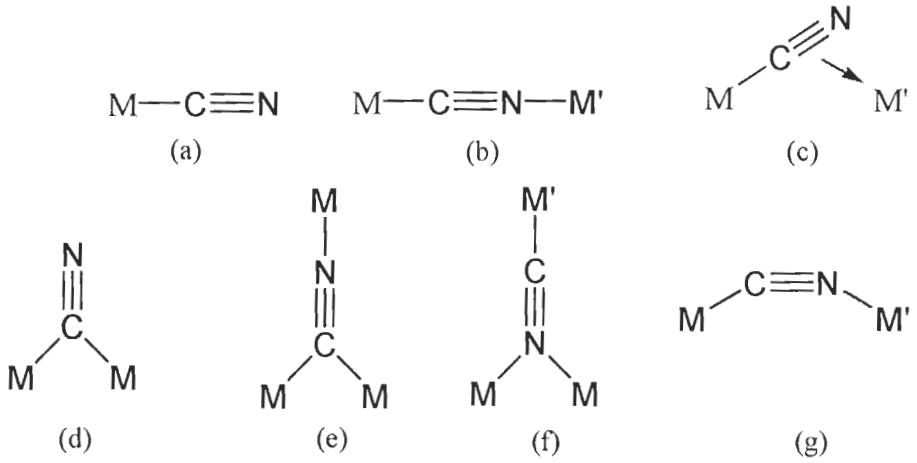

Figure 1-1: Terminal and bridging modes of the cyano group.

Cyanometallates can exhibit a variety of different geometries (Figure 1-2), exemplified by linear $[Ag(CN)_2]^-$, trigonal $[Cu(CN)_3]^{2-}$, tetrahedral $[Cd(CN)_4]^{2-}$, square planar $[Ni(CN)_4]^{2-}$, octahedral $[Fe(CN)_6]^{4-}$ and even seven or eight coordinated ones, all of which may behave as anionic building blocks to develop a variety of multidimensional structures.

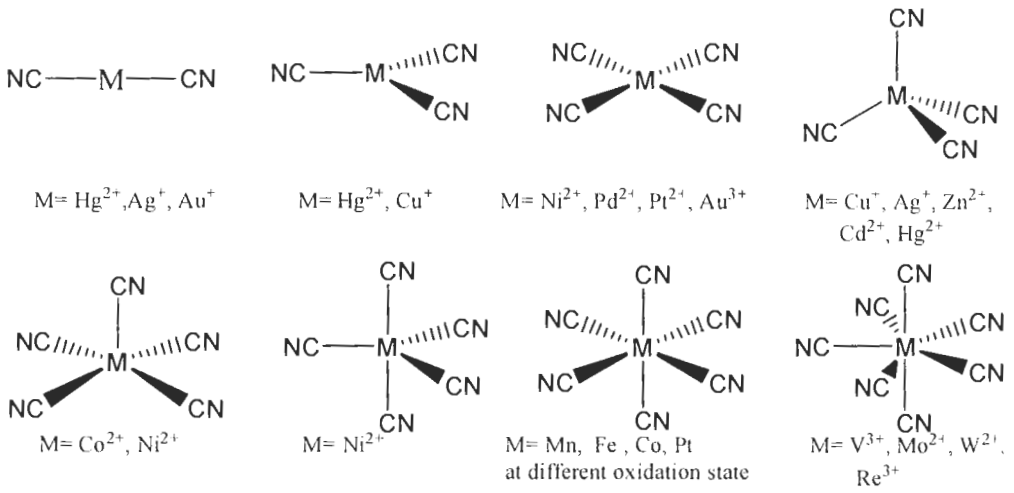

Figure 1-2: Observed geometries for common cyanometallates.

When a cyanometallate $[M(CN)_x]^{n-}$ is linked to another metal centre M', the linear M-CN-M' span is approximately 5 to 6 Å. The structure formed by successive M-CN-M' units can sometimes produce void space, which has the dimension to accommodate a guest molecule or ion with a suitable size. For this reason cyanometallate-based polymers are potential candidates for ion exchange, gas storage and sensor materials.[6]

1.1.3 Structures Derived from Square Planar and Tetrahedral $[M(CN)_4]^{n-}$

Four-coordinate square-planar cyanometallates, especially $[Ni(CN)_4]^{2-}$, have been extensively studied for their ability to support structurally diverse materials. Hofmann's benzene clathrate $[Ni(NH_3)_2Ni(CN)_4]$-$2C_6H_6$ is the first well-defined supramolecular structure of this type, which was first discovered in 1897.[5] These compounds are thus known as Hofmann-type clathrates with the formula of $[M'(NH_3)_2M(CN)_4]$-G, and they have a variety of guest molecules of certain sizes and shapes in their crystal lattice.[6]

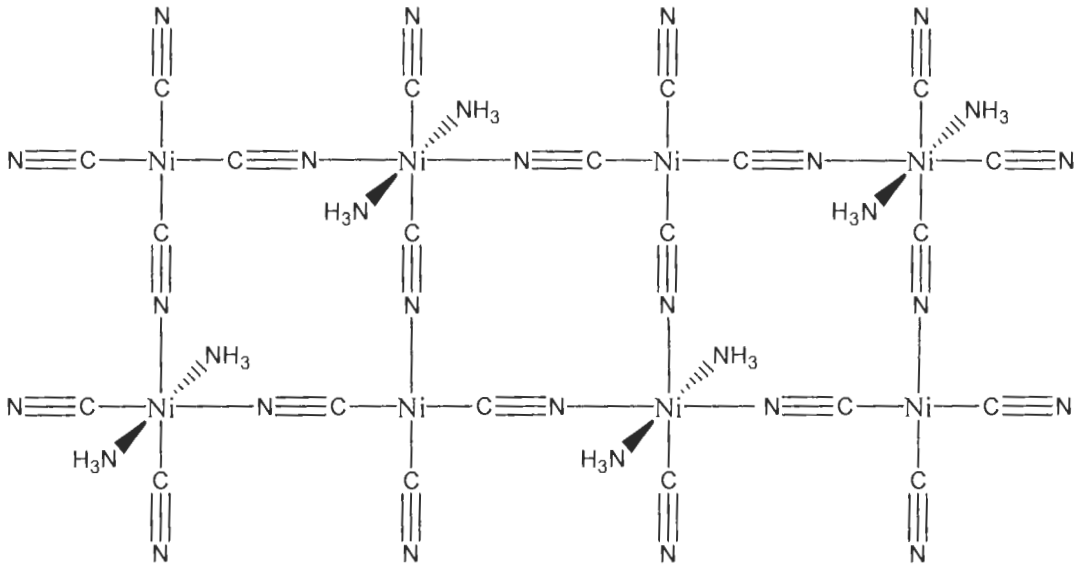

Figure 1-3: $Ni(NH_3)_2Ni(CN)_4$-$2C_6H_6$ – part of the 2-D Hofmann clathrate motif with square planar $Ni(CN)_4$ units and octahedral $Ni(NC)_4(NH_3)_2$. Benzene guest molecules are omitted for clarity.[7]

By replacing the square-planar d^8 $[M(CN)_4]^{2-}$ (M=Ni, Pd, Pt) with tetrahedral d^{10} $[Hg(CN)_4]^{2-}$ and $[Cd(CN)_4]^{2-}$, a vast diversity of modified Hofmann-type materials has been produced.[8] These compounds with $[Hg(CN)_4]^{2-}$ and $[Cd(CN)_4]^{2-}$ moieties have shown some limited use in constructing inclusion compounds that resemble SiO_2, clays and zeolite-cage structures.[6]

However, the related tetrahedral d^{10} building block $[Zn(CN)_4]^{2-}$ remains essentially unexplored and there are only a few reports of $[Zn(CN)_4]^{2-}$-based polymers. The focus of this thesis is to utilize $K_2Zn(CN)_4$ as a building block to construct coordination polymers. The unique properties of $[Zn(CN)_4]^{2-}$ and the resulting compounds will be discussed in latter parts of the thesis.

1.1.4 Structures Derived from Octahedral $[Fe(CN)_6]^{4-}$

Octahedral cyanometallates have been extensively employed to synthesize complexes related to the famous Prussian Blues (PBs). Other than their well investigated magnetic, electrochemical and ion-exchange properties,[3] the ability of PB to act as a gas storage material has been discovered recently.[9] Due to the open channel structure of PBs and a variety of combinations of metals in different oxidation states, more interest has been shown to the porosity of this system. In chapter three, two new Prussian Blue types of materials and their gas storage properties will be discussed in detail.

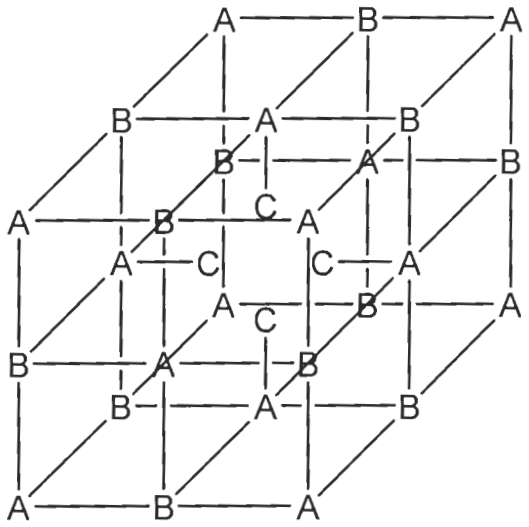

Figure 1-4: Prussian Blue. $Fe_4[Fe(CN)_6]_3$-$14H_2O$.

1.2 GENERAL TECHNIQUES

1.2.1 Coordination Polymer Preparation

Two apparent advantages of coordination polymers over other types of material are their ease of preparation and the mild reaction conditions. In general, a polar solution containing a metal ion (with or without a stoichiometric amount of additional capping ligand) is first prepared. Then a second solution containing the cyanometallate is added to the first solution with stirring. If an immediate precipitate is formed upon the mixing of the two solutions, then it is filtered (or centrifuged), washed, dried and characterized by a number of methods as described in Section 1.2.2. However, in cases where immediate precipitation does not occur, the solution is filtered, and then allowed to slowly evaporate in air at room temperature until a solid product (either microcrystalline powder or single crystals) is formed in the solution. The nature of solvent that is being used might be crucial for the structure of the final product since some solvents can act as a template in the crystallization process.[6, 8]

Although all of the crystals described in this thesis were prepared by slow evaporation, there are other methods of crystallization that can be used when a precipitate forms immediately upon mixing, including H-tube or agar-dish methods, where slow diffusion of the two reagent solutions is utilized.

1.2.2 Characterization Methods

1.2.2.1 Infrared Analyses

Infrared spectroscopy (IR) is a valuable method for characterization of supramolecular coordination polymers, and especially for cyanometallates. Generally, it is the first characterization performed on a product, in order to determine if any cyanometallate exists in the product. The terminal M-CN cyanometallate complexes exhibit distinctive peaks in the IR between 2000 and 2250 cm^{-1}, which have been intensively studied.[10] When a cyanometallate bridges to another metal centre, the cyanide stretches will shift from their non-bridge values. For most cases, a blue shift is observed when the cyanide bridges in the M-CN-M' mode due to donation of the lone pair electrons on the N atom, which is also weakly anti-bonding with respect to the CN triple bond, to the second metal centre M'.[3] In some cases, however, an increase in back bonding from M' to N can also occur, which results in a red shift for the cyanide stretching frequency νCN (Figure 1-5).[3] Furthermore, the number of distinctive νCN peaks is also indicative of the least number of structurally inequivalent cyanides in the product.

Infrared spectroscopy is also a valuable tool for determining the orientation of the cyanide in a M-CN-M' bridge. Typically, the original M-CN bond remains intact during reactions with other metals to produce linear bridges through the N atom, and the νCN of the bridging cyanide is largely dependent on the original νCN of M-CN. There are also examples where the direction of the CN

unit is switched to form M-N-C-M'; in those cases the νCN of the bridging cyanide is positioned closer to νCN of M'-CN rather than M-CN.[3]

Figure 1-5: Representation of cyanometallate σ-bonding (left) and π-back bonding (right).

1.2.2.2 Elemental and Thermogravimetric Analyses

If the IR spectrum suggests that cyanometallate moieties have been incorporated into products, an elemental analysis for the percentage of carbon, nitrogen and hydrogen is generally conducted, which gives useful information regarding product composition.

Depending on the system, sometimes more than one possible chemical formula can be deduced for one set of EA results. Thermo-Gravimetric Analysis (TGA), which measures the change in the weight of a sample as a function of temperature, becomes especially informative in this case since different types of ligand or solvent molecules in the crystal lattice have distinctive evaporation, decomposition or combustion temperatures. A precise determination of the empirical chemical formula can usually be obtained by combining the results of TGA with EA.

1.2.2.3 X-ray Crystallography

In order to definitively determine the solid state structure of the product, single crystal X-ray diffraction is vital. Although obtaining a suitable single crystal can be extremely difficult for some systems, X-ray crystallography is still the most powerful characterization tool and normally provides conclusive evidence of the product's structure. However, powder X-ray Diffraction can be employed when only the microcrystalline powder form of solid sample is available. The diffraction pattern then can be compared to those existing powder patterns in a database, and possibly indexed to yield useful structural information as well. [11] Differentiation between atoms of close nuclear charge (such as carbon and nitrogen, copper and zinc) can be difficult because those atoms have similar X-ray diffraction abilities.[11] It's common that X-ray data for cyanometallates with M-C-N-M' bridges cannot clearly differentiate the carbon and nitrogen atoms, and therefore the direction of the CN often remains unclear. This can be attributed to a poor quality single crystal or that the cyanide atoms are inherently disordered over the two positions. Similar limitations also apply to the polymers with disordered solvent molecules in that the position of the solvent atoms often cannot be precisely assigned.

1.2.2.4 Physical Properties

Once a polymer has been successfully prepared, a variety of physical property tests are performed, such as porosity, gas storage capacity, and magnetic susceptibility. Typically, studies are only performed after the polymer is characterized by IR, EA and X-ray Crystallography. Those results then guide the

examination of potential material properties. For instance, if the crystal structure of the product shows accessible cavities and channels, then the porosity and surface area of the polymer is probed using nitrogen and other gas adsorption isotherm measurements. If magnetic coupling appears to be possible, then the magnetic susceptibility of the material as a function of temperature will be measured using a SQUID magnetometer.

1.3 RESEARCH OBJECTIVE

The general purpose of this thesis is to examine the use of $[Zn(CN)_4]^{2-}$ as a building block in the preparation of supramolecular coordination polymers. Attention is given to the factors that influence the crystal structure of the products and their porosity such as the presence or absence of templating cations and/or solvent molecules, the changes of ancillary capping ligands (if any) and the identity of the second metal cation. Also of interest are the resulting physical properties of the supramolecular system, e.g. gas storage and solvent detection.

CHAPTER 2: TETRACYANOZINCATE AS A SUPRAMOLECULAR BUILDING BLOCK

2.1 INTRODUCTION

As mentioned in Chapter 1, some work has been done regarding the application of the d^{10} tetrahedral building blocks $[Cd(CN)_4]^{2-}$ and $[Hg(CN)_4]^{2-}$. Given this, it is surprising that there are so few reported coordination polymers using the analogous tetrahedral building block $[Zn(CN)_4]^{2-}$.[12,14] In 1990, Hoskins and Robson first reported the tetracyanozinc compound, 3-D zincblende-type $[N(CH_3)_4][Cu^{I}Zn^{II}(CN)_4]$, that contains structural space for the inclusion of the $N(CH_3)_4^+$ cations.[12] It was later characterized by solid state ^{13}C MAS NMR in order to distinguish which metal was C-bound, and it turned out that all of the zinc centres are nitrogen-bonded to form a chain of Cu-C-N-Zn; in other words, the cyanides flipped direction upon reacting with Cu(I).[13] To date, the only reported example that shows a tetrahedral ZnC_4 connectivity is $[Zn(pyridine)_2][Zn(CN)_4]$ where the cyanide bridges between two zinc centres.[14] This limited number of examples displays the difficulty of utilizing this building block.

One reason for the paucity of reported d^{10}-$[Zn(CN)_4]^{2-}$-based coordination polymers in general may lie with the relatively low stability of aqueous $K_2[Zn(CN)_4]$, which has an overall aqueous formation constant $\beta_4=3.7*10^{21}$ M^{-4}. Although not particularly labile ($KZn(CN)_3 + KCN \rightarrow K_2[Zn(CN)_4]$, $K_4= 7.7*10^4$ M^{-1})

[15,16], when $[Zn(CN)_4]^{2-}$ is reacted with other metals with a higher cyanide-affinity, some or all of its bound cyanide groups are released upon interacting with the other metal present. In the case of $[Zn(pyridine)_2][Zn(CN)_4]$, the companion metal is another Zn(II) centre, obviating any competing formation constant or lability issues. [14]

In order to solve this stability problem of $[Zn(CN)_4]^{2-}$ and incorporate it into coordination polymers, this thesis considered the choices of the companion metals and ligands. Since the two coordination reactions between the second metal and free cyanides or other ligands are competing processes, chelating ligands were utilized to react with (and protect) the second metal centres. Sometimes, a higher concentration of ligands is necessary in order to compete with free cyanide reactions. In addition, the oxidation state of the second metal is another factor to consider, as cyanide has a certain degree of reducing ability. Different types of solvents other than water were also tried in the hope that $[Zn(CN)_4]^{2-}$ may be less labile and react differently in non-aqueous solution, although the solubility of $K_2Zn(CN)_4$ needed to be considered. Mixtures of solvents with different ratios or even immiscible solvents were also experimented to test the stability of $[Zn(CN)_4]^{2-}$ in them or at the interface of two immiscible solvents. Among all of the companion metals and ligands that were tried, ethylenediamine turned out to be a particular effective protecting ligand when used in excess, and copper(II)/(I) with their modest cyanide affinity together with $[Zn(CN)_4]^{2-}$ afforded some interesting coordination polymers, which will be described in the following sections.

2.2 RESULTS AND DISCUSSION

2.2.1 Synthesis and Characterization of $[Cu(en)_2][Zn(NC)_4(CuCN)_2]$ (2.1)

The addition of an aqueous solution of $K_2[Zn(CN)_4]$ (1 equiv.) to an aqueous solution of $Cu(ClO_4)_2 \cdot 6H_2O$ (1 equiv.) containing three equiv. of ethylenediamine (**en**) produced dark purple crystals of **2.1** overnight. If the reaction is performed with two or fewer equiv. of **en**, the dark blue Cu(II) solution completely decolorizes.[17] The IR spectrum of **2.1** in the νCN region shows six different peaks, indicating an unexpected structural complexity. Indeed, the X-ray crystal structure of **2.1** reveals the formation of a mixed-valent Cu(I)/Cu(II)/Zn(II) polymer with the formula $[Cu(en)_2][Zn(NC)_4(CuCN)_2]$ (**2.1**) and six inequivalent cyanide groups. The anionic $[Zn(NC)_4(CuCN)_2]^{2-}$ moiety forms a 2-D puckered sheet and the $[Cu(en)_2]^{2+}$ cations lie in the cavities between and within the sheets, perhaps templating their formation (Figure 2-1).[18]

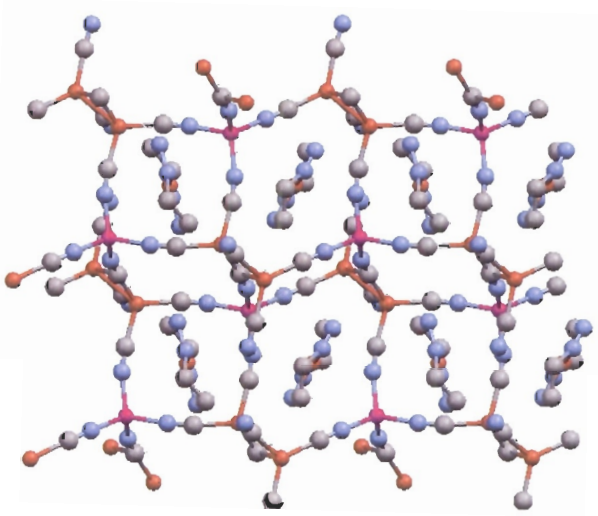

Figure 2-1: Polymer 2.1 viewed along the b-axis, showing the anionic 2-D array of $[Zn(NC)_4(CuCN)_2]^{2-}$ and embedded $[Cu(en)_2]^{2+}$ cations. Colour scheme: Cu, orange; Zn, pink; C, gray; N, blue. Hydrogen atoms were omitted for clarity.

The axial sites of the paramagnetic $[Cu(en)_2]^{2+}$ are unligated; the closest contact is the N-terminus of cyanide CN(10) at 2.73 and 2.95 Å from the two $[Cu(en)_2]^{2+}$ in the unit cell. Within the anionic cyanometallate layer, the two Cu(I) centers have four-coordinate, distorted tetrahedral geometries (Figure 2-2).

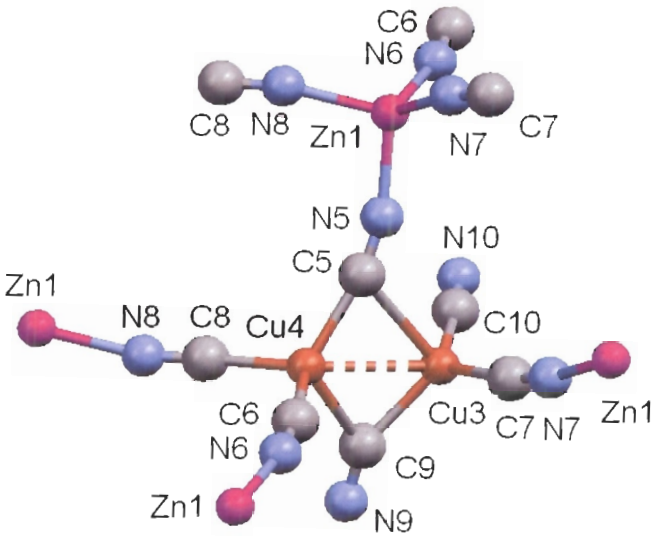

Figure 2-2: Detailed structure of anionic layer $[Zn(NC)_4(CuCN)_2]^{2-}$ with numbering scheme. Selected bond lengths (Å): Zn(1)-N(5) 1.985(4), Zn(1)-N(6) 1.976(4), Zn(1)-N(7) 1.960(4), Zn(1)-N(8) 1.966(4), Cu(3)-C(5) 2.493(5), Cu(3)-C(7) 1.936(4), Cu(3)-C(9) 2.025(5), Cu(3)-C(10) 1.935(5), Cu(4)-C(5) 1.970(5), Cu(4)-C(6) 1.970(5), Cu(4)-C(8) 1.959(5), Cu(4)-C(9) 2.237(5), Cu(3)-Cu(4) 2.6458(10).

All CN- groups are C-bound to the Cu(I) centers, which build a dinuclear $[Cu_2(CN)_6]^{4-}$ cyanide-bridged cluster within the 2-D array, with a Cu(3)-Cu(4) distance of 2.6458(10) Å - well within the range for reported "cuprophilic interactions".[19,20] Three of the cyanides (CN6,7,8) are μ_2-bridging to a Zn(II) center, and the fourth cyanide (CN5) μ_3-bridges from two Cu(I) centers to the Zn(II) node. Thus, the Zn(II) metal center is also tetrahedrally coordinated but is N-bound to four cyanides rather than to the C-bound cyanides as in the starting

material $[Zn(CN)_4]^{2-}$, which does not survive the reaction conditions. The direction of the cyanide binding (C-terminus on Cu(I) vs. Zn(II)) was determined by X-ray crystallography (IR spectra are also definitive; see below); By flipping the cyanide direction from Zn-CN-Cu to Zn-NC-Cu in the single crystal structure, the R value was reduced from 0.050 to 0.039, which suggested that the latter configuration (Zn-N-C-Cu) was more likely to be correct. It was also confirmed by MAS Solid State NMR spectroscopy. A comparison of the actual ^{13}C and ^{15}N peak widths with the known coupling constants between Zn/Cu and C/N ruled out the possibility of any N-Cu or Zn-C interactions.[21] In the related 3-D zincblende-type $Me_4N[ZnCu(CN)_4]$ polymer, the switch in CN-directionality from Zn-CN-Cu to Zn-NC-Cu was also and could only be determined by MAS NMR techniques due to disordered metal and cyanide sites.[12,13] Regarding the two remaining Cu(I)-cyanide ligands in the structure: C9-N9 forms a μ_2-C-bridge between the two Cu(I) centers, thereby supporting the dicopper(I) cluster, and C10-N10 is terminal to Cu(3). Thus, there are six inequivalent CN groups, sporting four different binding modes in one compound! Although various cyanide binding modes have been reported in other systems,[22] the simultaneous existence of such a diverse range in a single complex is remarkable.

This variation in CN-bonding is reflected in six νCN peaks at 2136, 2128, 2111, 2089, 2082 and 2067 cm^{-1}; these are all red-shifted compared to the 2153 cm^{-1} of $K_2[Zn(CN)_4]$ but generally blue-shifted relative to $K_3[Cu(CN)_4]$ (2075, 2081, 2094 cm-1),[15] consistent with the change to C-bound Cu(I) centers, as νCN peaks usually blue-shift upon binding of the M-CN N-terminus to a second

metal.[3,6,23] For comparison, the νCN peak for the Cu(I)-CN-Zn(II) moiety in $Me_4N[ZnCu(CN)_4]$ is observed at 2130 cm^{-1}. Also, the μ_2-C-bridging cyanides in $(CuCN)_2$ dimer groups in a series of diamine-CuCN polymers[20] are found between 2045-2080 cm^{-1}, red-shifted relative to terminal Cu-CN groups in three- or four-coordinate Cu(I) systems. In this light, the lowest vibration for **2.1** is likely the μ_2-C-bridging CN9 and the three highest vibrations probably correspond to μ_2-Cu/Zn bridging units; the terminal and μ_3-bridging cyanides are difficult to differentiate due to competing red- and blue-shifting factors for the μ_3-CN5.

At 300 K, the μ_{eff} for **2.1** is 1.8 μ_B and it obeys the Curie-Law (μ_{eff} is independent of temperature) down to 10 K, consistent with the presence of isolated copper(II) centers. Despite this paramagnetism, ^{13}C and ^{15}N MAS NMR spectra were successfully recorded at natural isotopic abundance by Pedro Aguiar and Prof. Scott Kroeker (University of Manitoba).[21]

The facile release of cyanide from $[Zn(CN)_4]^{2-}$ is likely also responsible for the presence of Cu(I) in **2.1** in the first place. It is well-known that CN^- reacts with aqueous Cu(II) to generate Cu(I) and cyanogen and that this reaction is attenuated by amine-ligation to Cu(II);[17,24,25,26] in this light, the mechanism for Cu(I) generation as well as the requirement for three equiv. of en both become clear. If only two equivalents of **en** are used, the Cu(II) will still be reduced to Cu(I), causing the observed decoloration. This reaction has been used more directly (i.e. addition of CN^- to a Cu(II) solution) to generate cyanide-bridged mixed-valent Cu(I)-Cu(II) coordination polymers in which the size of templating neutral molecules or cations play a crucial role in determining the structure and

CN-binding modes;[17,24,25] many cyanocuprate(I) polymers have also been reported from the direct reaction of CuCN/CN^- and nitrogen-based ligands.[20,27,28] The synthesis of bimetallic **2.1** is more complicated since, in the reaction of Cu(II)/en and $K_2Zn(CN)_4$, the latter acts both as an indirect reducing agent (via its CN^-) and as a source of Zn(II) and CN^- units.

2.2.2 Solvent Templated Derivative: Synthesis and Characterization of $[Cu(en)_2]_{0.5}[CuZn(NC)_4][C_6H_5Cl]_n$[1] (2.2)

Since the first cyanometallate clathrate-Hofmann's benzene clathrates was synthesised more than a century ago,[5] plenty of studies have been done on clathrates and the effect of solvents molecules in templating crystal structures and tuning their physical properties. [6,8] By replacing the square planar $Ni(CN)_4$ in the Hofmann type clathrates by tetrahedral $M(CN)_4$ (M=Cd, Hg), many interesting structures were generated, with different types of solvents entrapped.[6] Interestingly, a number of the $Cd(CN)_2$ host and analogous clathrates like $CdM(CN)_4$-2G (M = Hg, Zn) exhibit similar structures with those of SiO_2 when different solvent molecules are included in the structure.[29]

In the synthesis of coordination polymers, sometimes solvents can play a crucial role in the structure of product crystals by incorporating the solvent molecules themselves inside. The different types of solvents also have different physical properties for the reactants, such as solubility, miscibility, and polarity, which may eventually change the lability of the reactant (e.g. $K_2[Zn(CN)_4]$), or mechanism of the reaction. Thus, after carrying out the preparation procedure of

[1] The proposed formula of 2.2 is based on the results of IR and partially solved X-ray data, which does not exactly match the elemental-analysis results. More details in experimental.

2.1 by the addition of an aqueous solution of $K_2[Zn(CN)_4]$ (1 equiv.) to an aqueous solution of $Cu(ClO_4)_2 \cdot 6H_2O$ (1 equiv.) containing three equiv. of ethylenediamine (en) to produce a dark purple aqueous solution as before, this time a layer of chlorobenzene was added underneath the aqueous solution while stirring. A new product, different than **2.1**, in the form of some rod-shaped blue crystals with hexagonal bases or ends were afforded from this mixture after one week. The IR spectrum of **2.2** in the νCN region showed one peak, indicating an unexpected structural simplicity, compared with **2.1**, which is obtained without the chlorobenzene layer.

The reaction has been repeatedly carried out following the same procedures described above, and several crystals suitable for single crystal X-ray studies were obtained. They all share the same rod-like shape with a perfect hexagonal base or end, although under a polarized microscope the whole crystal does not lighten and darken at the same time, but follows an alternating manner. This suggested significant twinning during crystal growth. In order to obtain a single piece, all the crystals needed to be cut into homogeneous pieces, although some degree of twinning is quite hard to avoid, especially along the c-axis (assuming it has a hexagonal unit cell).

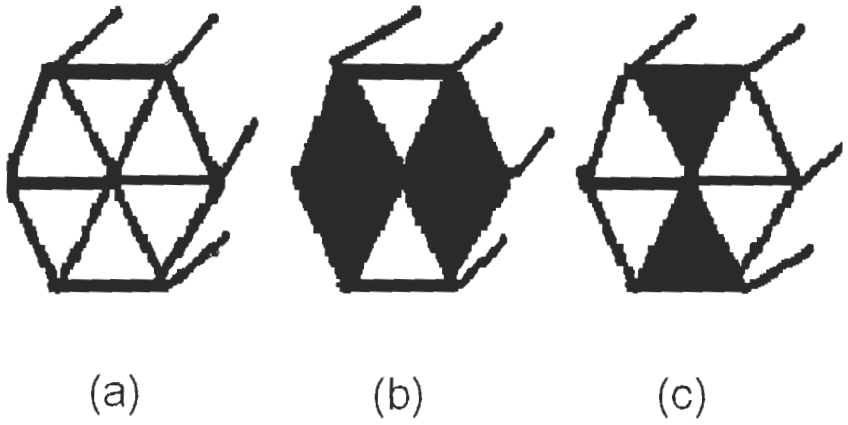

Figure 2-3: Base sections of crystals of compound 2.2 under polarized microscope lighten and darken following an alternating manner. A) Under normal light; B) Under polarized microscope; C) Under polarized microscope, another direction.

From the crystals of **2.2** that were obtained from the above reaction, the crystal structure was only partially solved due to a combination of the twinning problems and disordered solvent molecules in the structure.[2] Several different data sets each yielded different, but related unit cells; de-twinning software was not useful. Despite this, solutions from the data obtained were sufficient to reveal some information about the identity of the compound, as well as its atomic connectivity.

Following are two solutions from crystal data of **2.2**. The first one (Figure 2-4, Figure 2-5) was collected and solved in a higher symmetry (P 6_3 m c, hexagonal) than the second one (A m m 2, Orthorhombic) (Figure 2-6, Figure 2-7). The cells are outlined in the figures.

[2] The single crystal structures of compound **2.2** and **2.3** were solved and refined by Mr. Michael J. Katz.

Table 2-1: Crystallographic data for 2.2. Two related solutions in different space groups. $a_2 \approx c_1$; $b_2 \approx 3a_1$; $c_2 \approx 2\sin 60^\circ a_1$.

	Solution 1	Solution 2
Space group	$P6_3mc$	Amm2
a, Å	8.3400	13.2816
b, Å	8.3400	25.0230
c, Å	13.2340	14.4510
α, deg	90	90
β, deg	90	90
γ, deg	120	90
R, Rw	0.249, 0.187	0.102, 0.142

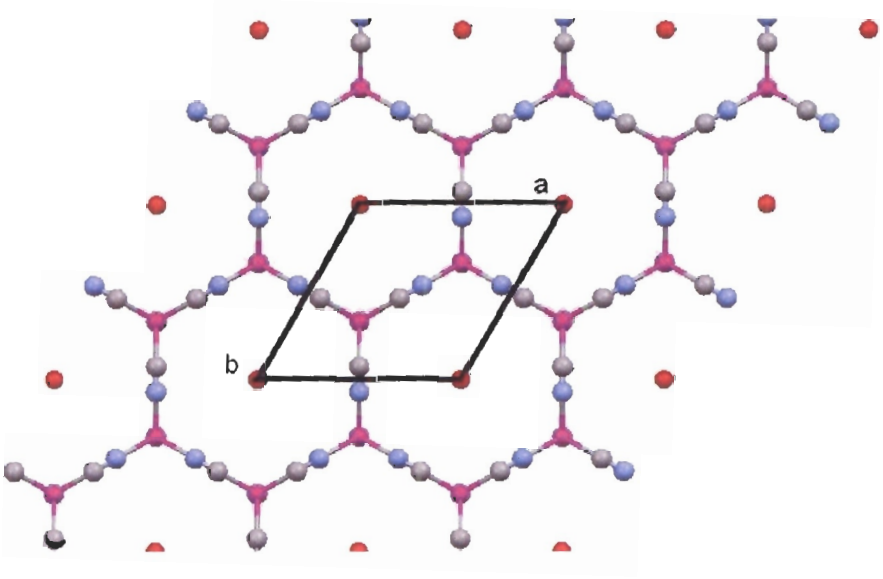

Figure 2-4: Partially solved crystal structure of compound 2.2 in $P6_3mc$, viewed along the C axis. The red dot represents the unsolved components in the (hexagonal) adamantane-diamond shaped $CuZn(CN)_4$ network. Colour scheme: Cu, orange; Zn, pink; C, gray; N, blue.

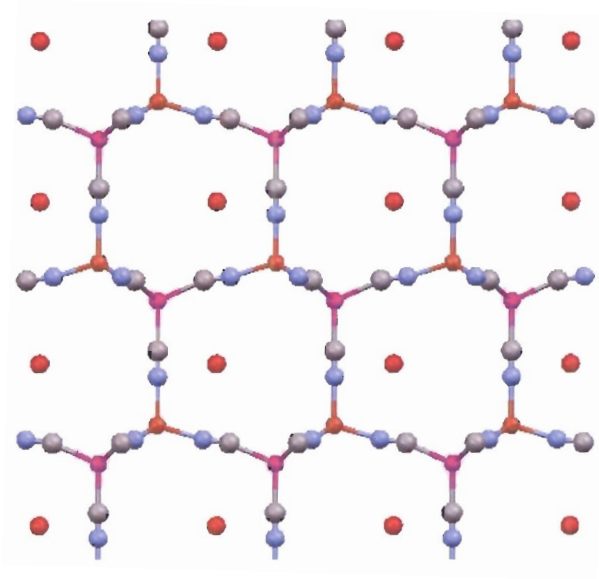

Figure 2-5: Partially solved crystal structure of compound 2.2 in $P6_3mc$, viewed along the a-axis. The red dot represents the unsolved components in the (hexagonal) adamantane-diamond shaped $CuZn(CN)_4$ network. Colour scheme: Cu, orange; Zn, pink; C, gray; N, blue.

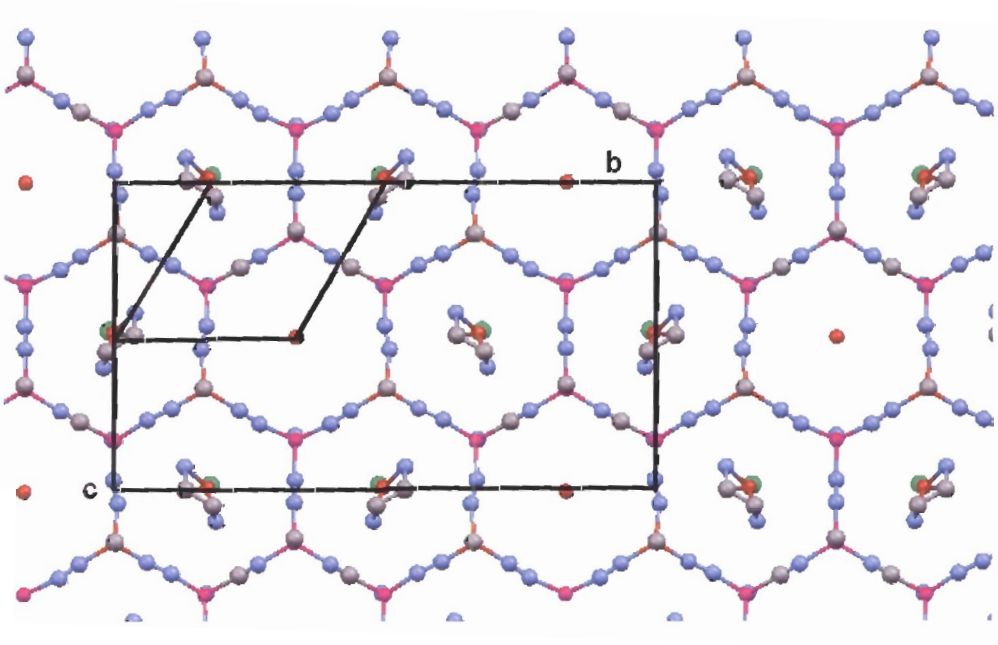

Figure 2-6: Partially solved crystal structure of compound 2.2 in Amm2, viewed along the a axis. Colour scheme: Cu, orange; Zn, pink; C, gray; N, blue; Cl, green. No chlorobenzene was observable. The hexagonal and A centred orthorhombic cells are shown.

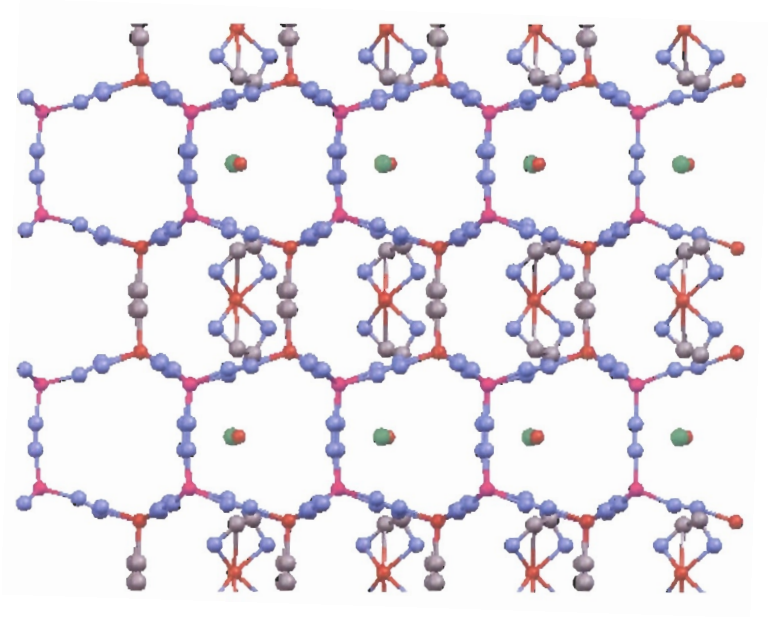

Figure 2-7: Partially solved crystal structure of compound 2.2 in Amm2, viewed along the b axis. Colour scheme: Cu, orange; Zn, pink; C, gray; N, blue; Cl, green. No chlorobenzene was observable.

As shown in the above figures, the basic 3-D framework is very similar no matter what solution is used; one distortion of a cyanide group (or contents in the cavities) can easily eliminate the 6-fold symmetry and transform the unit cell to orthorhombic. Indeed, the lower symmetry cell is more likely to be more correct. The main framework of the compound is an adamantane-shaped $[CuZn(CN)_4]^-$ 3-D anionic network, which probably accounts for the hexagonal shaped base and end in the bulk crystals. The contents of the cavities are not clearly defined in the crystal structures. A $[Cu(en)_2]^{2+}$ unit and some chlorobenzene molecules are the suspected candidates that fill the cavities, since both of them are detected by IR, and the blue color of the crystal shows the existence of copper 2+ ions. Although the $[Cu(en)_2]^{2+}$ units can be identified in the Amm2 structure, chlorobenzene is not observed, likely due to a combination of disorder and high

thermal motion. In both of the solutions, atoms with similar diffraction power (Cu/Zn or C/N) can not be clearly differentiated from each other with the data set. They may be fundamentally disordered as well.

Due to the high R-values, disorder and twinning, any bond lengths and angle data would have large uncertainties and thus have not been listed or used as a basis for discussion.

A comparison of powder diffraction spectra of compound **2.2** both the calculated one from the single crystal structure (Amm2) and the experimental diffractogram, are shown below. Most of the peaks for the calculated PXRD match the experimental data well, which suggests that the main framework of $[CuZn(CN)_4]^-$ does indeed exist in the structure. Another compound with similar structure was also synthesised in the same way, by replacing chlorobenzene by 1,2-dichloroethane (ClC_2H_4Cl) in the mixing step of the synthesis ($[Cu(en)_2]_{0.5}[CuZn(NC)_4][ClC_2H_4Cl]_n$, **2.2a**). The PXRD of 2.2a shows similar major peaks in the spectra. This compound is not discussed in detail in this thesis because of the lack of other supporting information.

Attempts have been made to replace the chlorobenzene solvent or even simply remove it from the structure. However, after removing the chlorobenzene molecules by heating to 150 °C, the framework does not maintain its rigidity and it goes through an irreversible structure change (indicated by drastic changes of IR cyanide peaks, from one peak at 2116 cm^{-1} to two peaks at 2120 and 2163 cm^{-1}). Even immersing the resulting grey solid in chlorobenzene solvent (or $CHCl_3$), the initial **2.2** network is not regenerated.

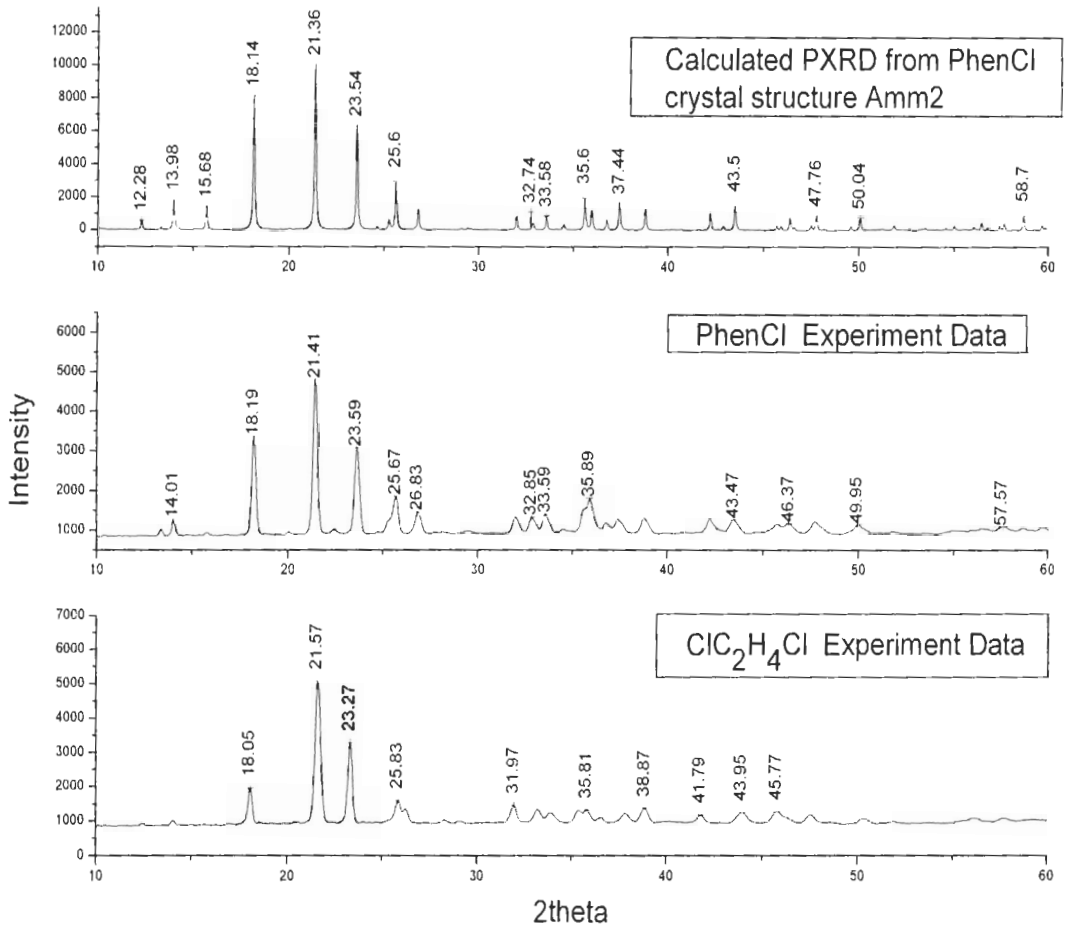

Figure 2-8: Powder Diffraction Spectrum for A) Compound 2.2, spectrum generated from crystal X-ray data (top); B) Compound 2.2(middle); C) Crystals with ClC_2H_4Cl solvent (bottom).

2.2.3 Solvent Templated Derivative: Synthesis and Characterization of $[Cu(en)_2]_{0.5}[CuZn(NC)_4](CHCl_3)$ (2.3)

Following the method as used for **2.2**, with the use of $CHCl_3$ instead of chlorobenzene solvent, **2.3** was formed as blocks of dark red crystals. The IR spectrum of **2.3** in the νCN region shows three peaks, indicating a less-symmetric network formed.

The X-ray crystal structure of **2.3** reveals the formation of a Cu(I)/Zn(II) network with the formula $[ZnCu(NC)_4]_n$, although it's of lower symmetry than the

almost perfect adamantane-diamond like structure that **2.2** has. The anionic $[ZnCu(NC)_4]^-$ moiety forms a 3-D network and all the metals are four-cyanide-coordinated. $[Cu(en)_2]^{2+}$ cations and chloroform molecules lie in the cavities , perhaps templating the formation of this network and distorting it from the higher symmetry observed in **2.2**. The cyanides are not crystallographically equivalent, which is consistent with the IR spectrum showing multiple νCN peaks. Chloroform molecules are not definitively positioned in the structure because of the combination of disorder and thermal motion. The interaction between the Cu(II) centre in the $[Cu(en)_2]^{2+}$ unit and the chlorine atoms in chloroform may have shifted the visible absorption spectrum of the Cu(II) centre, causing the red color of this compound, instead of the normal purple-blue-green color of the $[Cu(en)_2]^{2+}$ unit.

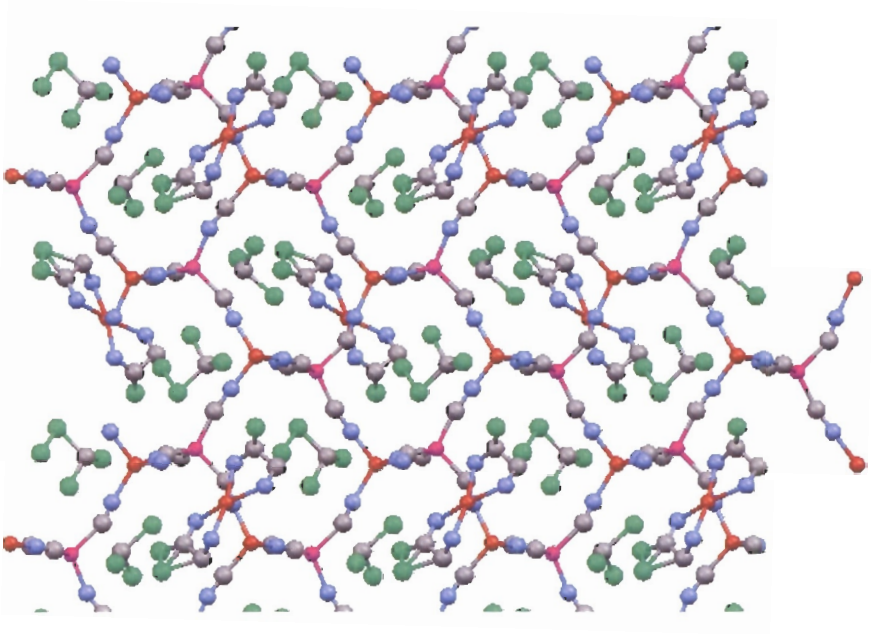

Figure 2-9: Crystal structure of compound 2.3, viewed along a axis in a monoclinic cell. Colour scheme: Cu, orange; Zn, pink; C, gray; N, blue; Cl, green.

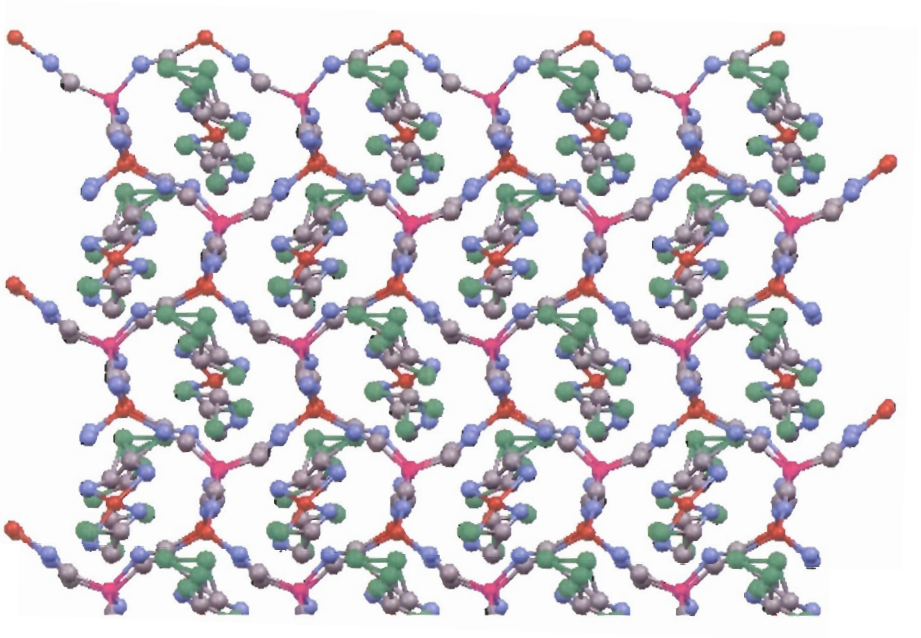

Figure 2-10: Crystal structure of compound 2.3, viewed along c axis in a monoclinic cell. Colour scheme: Cu, orange; Zn, pink; C, gray; N, blue; Cl, green.

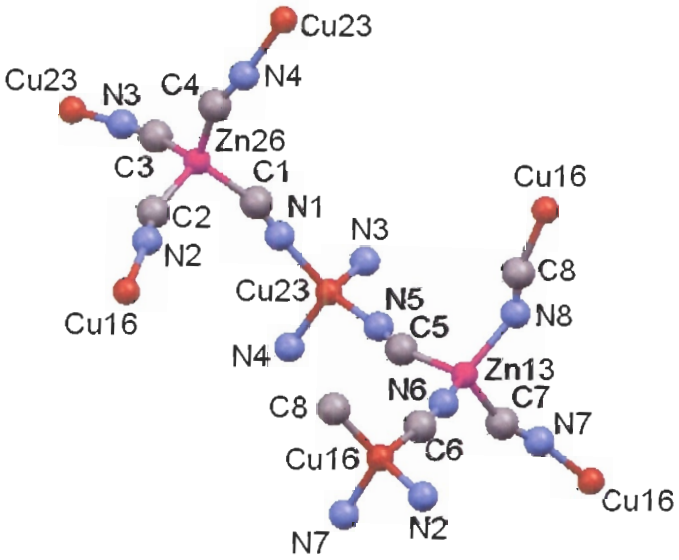

Figure 2-11: Structure of compound 2.3, showing only the $[CuZn(CN)_4]_2^{2-}$ unit.

Table 2-2; Selected Bond Lengths (top) and Angles (bottom) for compound 2.3

Selected	Atoms	Bond Length	Selected	Atoms	Bond Length
Zn13	N6	1.95(4)Å	Zn13	N8	2.08(4)Å
Zn13	C5	1.99(5)Å	Zn13	C7	1.95(4)Å
Zn26	C1	1.93(5)Å	Zn26	C2	2.03(5)Å
Zn26	C3	1.91(5)Å	Zn26	C4	1.91(5)Å
Cu16	N2	2.00(4)Å	Cu16	N7	1.94(4)Å
Cu16	C6	1.92(5)Å	Cu16	C8	1.90(5)Å
Cu23	N1	2.07(4)Å	Cu23	N3	1.87(4)Å
Cu23	N4	1.94(4)Å	Cu23	N5	2.00(4)Å
N1	C1	1.10(5)Å	N2	C2	1.08(5)Å
N3	C3	1.26(5)Å	N4	C4	1.23(5)Å
N5	C5	1.07(5)Å	N6	C6	1.20(5)Å
N7	C7	1.22(5)Å	N8	C8	1.20(5)Å

Selected	Atoms		Angle	Selected	Atoms		Angle
N6	Zn13	N8	107.9(14)°	N6	Zn13	C5	110.7(17)°
N8	Zn13	C5	109.6(16)°	N6	Zn13	C7	114.3(17)°
N8	Zn13	C7	106.1(17)°	C5	Zn13	C7	108.2(18)°
N2	Cu16	N7	101.6(15)°	N2	Cu16	C6	113.8(18)°
N7	Cu16	C6	102.4(17)°	N2	Cu16	C8	111.1(17)°
N7	Cu16	C8	114.7(18)°	C6	Cu16	C8	112.5(19)°
N1	Cu23	N3	106.8(15)°	N1	Cu23	N4	112.4(16)°
N3	Cu23	N4	102.7(15)°	N1	Cu23	N5	116.4(15)°
N3	Cu23	N5	111.3(16)°	N4	Cu23	N5	106.5(15)°
Cu23	N1	C1	175(4)°	Cu16	N2	C2	173(4)°
Cu23	N3	C3	177(3)°	Cu23	N4	C4	171(3)°
Cu23	N5	C5	172(4)°	Zn13	N6	C6	163(4)°
Cu16	N7	C7	170(4)°	Zn13	N8	C8	141(4)°
Zn26	C1	N1	161(4)°	Zn26	C2	N2	154(5)°
Zn26	C3	N3	170(4)°	Zn26	C4	N4	156(4)°
Zn13	C5	N5	160(5)°	Cu16	C6	N6	175(4)°
Zn13	C7	N7	158(4)°	Cu16	C8	N8	162(4)°

The powder diffraction pattern of **2.3** is shown in Figure 2-12, and compared with the powder pattern generated from the single crystal structure.

Many of the peaks correspond, although with different relative intensity, but a significant portion of the peaks do not, indicating some degree of uncertainty in the crystal structural solution. This is perhaps due to the loss of chloroform molecules from the crystal structure during the grinding process from single crystals into powder. The disordered solvent molecules (chloroform) were also a possible cause of this difference.

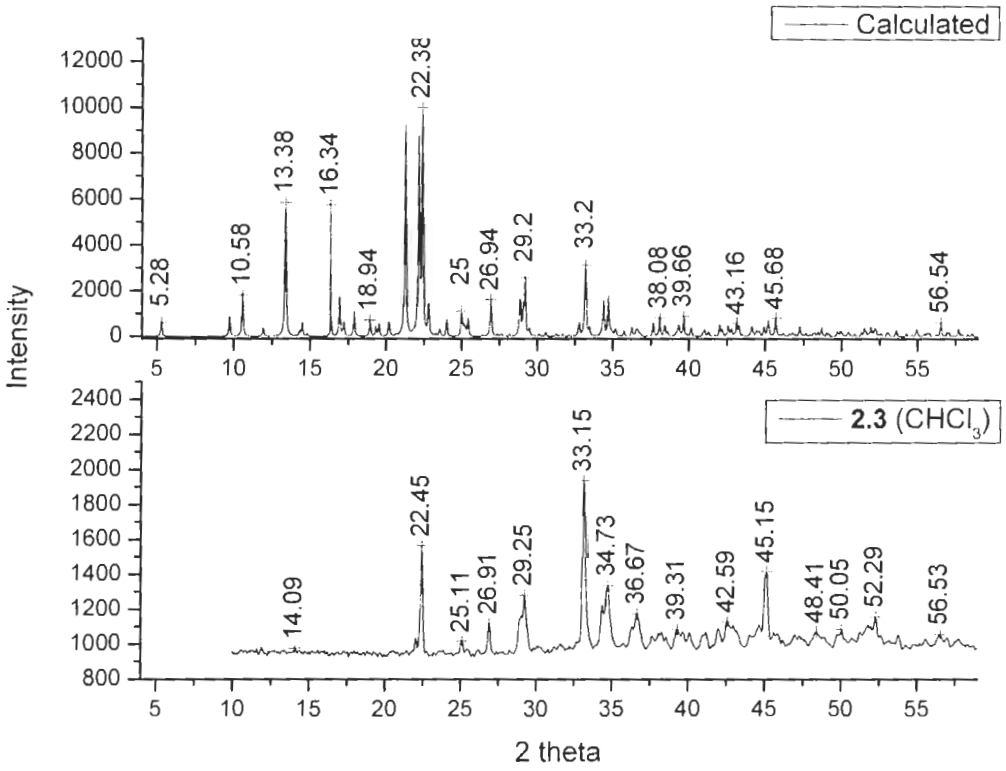

Figure 2-12: Powder Diffraction pattern for A) Compound 2.3 pattern generated from single crystal X-ray data (top); B) Compound 2.3 experimental powder diffraction pattern of grind crystals (bottom).

Irreversible structure changes also occurred when crystals of **2.3** were heated to 180 °C to remove the solvent (from three peaks of 2152, 2125, 2112

cm^{-1} to one peak at 2137 cm^{-1}), accompanied by a colour change to blue and then grey. The $CHCl_3$-free grey compound can not reabsorb the solvent even after immersion in $CHCl_3$, indicating an irreversible structure change.

2.2.4 Synthesis and Characterization of $[Ni(en)_2][Ni(CN)_4]$-2.16H_2O (2.4)

In an attempt to form similar compounds with Ni(II) in place of Cu(II) without the redox problem of copper ion, the reaction of a methanol/water solution containing 1 equivalent of $Ni(NO_3)_2 \cdot 6H_2O$ and 6 equivalents of ethylenediamine (en) with a methanol solution of 2 equivalents of $K_2Zn(CN)_4$ produced no immediate precipitate. Upon leaving the resulting green solution, covered and undisturbed for 3 days, purple crystals of $[Ni(en)_2][Ni(CN)_4]$-2.16H_2O (**2.4**) with different sizes were deposited from the solution, differentiated and separated manually under the microscope. Single crystal X-ray analysis revealed that the crystals with different sizes have two different crystal structures; both are previously reported structures found by J. Cernak et al, in 1990.[30] The smaller purple crystals are the trans- $[Ni(en)_2][Ni(CN)_4]$-2.16H_2O (**2.4.1**), and the larger crystals are cis-$[Ni(en)_2][Ni(CN)_4]$-2.16H_2O **(2.4.2)**. Not having any cyano-zinc moieties in these two compounds is disappointing considering the goal of this project was to incorporate $Zn(CN)_4^{2-}$ into the structure of a polymer, however, it's certainly not surprising or unique for Ni^{2+} to easily extract cyanides to form stable complexes, since the formation constant β_4 for d^8-$[Ni(CN)_4]$ is *ca.* 10^{10} larger than that for the zinc-analogue.[15] It also suggests that cyanides on the $Zn(CN)_4^{2-}$ could be labile.

2.2.5 Synthesis and Characterization of $[Ni(dien)Ni(CN)_4]_n$-$(H_2O)_n$ (2.5)

Following the method as used for **2.4**, with the use of 2 equivalents of diethylenetriamine (**dien**) instead of 3 equivalents of **en**, purple crystals of $[Ni(dien)Ni(CN)_4]_n$-$(H_2O)_n$ (**2.5**) was deposited from solution after a week. The crystal structure of **2.5** was reported by Inaki Muga et al in 2004.[31] Once again, tetrahedral $[Zn(CN)_4]^{2-}$ did not survive the reaction with Ni^{2+}, and only acted as a source of cyanide to generate $[Ni(CN)_4]^{2-}$.

2.2.6 Other Endeavours with the $[Zn(CN)_4]^{2-}$ Building Block

Over 20 reactions were conducted with a combination of the following components in either water or methanol solutions: Metals: Cu^{2+}, Mn^{2+}, Co^{2+}, Fe^{3+}; Ligands (2 or 3 equiv.): **en**, **dien**, **tren**, **bipy**, **phen**; and the required amount of $K_2Zn(CN)_4$ to balance the transition metal charge. A representative experimental is the same method for preparing **2.1**. The lability of the $[Zn(CN)_4]^{2-}$ and the reducing property of free cyanide made these experiments complicated. The νCN stretches in the infrared spectra of the resulting products showed a trend of blue shift compared with $[Zn(CN)_4]^{2-}$ (2153 cm^{-1}), CuCN (2116 cm^{-1}), $Zn(CN)_2$ (2200 cm^{-1}) or other similarly common metal cyanide by-products. Many of the products showed visible impurities and it is difficult to confidently suggest their composition. Furthermore, the preparation of X-ray quality crystals was not successful and thus these reactions were not pursued further.

2.3 CONCLUSIONS AND FUTURE WORK

$K_2Zn(CN)_4$ has been used as a starting material in order to incorporate the

$Zn(CN)_4^{2-}$ building block into coordination polymers. Due to its lability, it turns out to be a useful reducing agent and cyanide source when reacted with other metals. Although none of the resulting products contains the $[Zn(CN)_4]^{2-}$ building block as intended, some of the structures are also very interesting and unique. Compound **2.1** with a Cu(I)/Cu(II)/Zn(II) mixed-valent network showed a 2-D structure with six structurally inequivalent cyanides in four distinct bonding modes. Chlorinated solvents were also utilized in order to template the existing structures to make compound **2.2** and **2.3** with diamond-shaped anionic $[ZnCu(CN)_4]_n^{n-}$ networks. Although no reversible solvent removal was achieved, the potential to do so has not been disproven. For example, the blue product when **2.3** is heated and the end-resulting grey powders needs to be further characterized. Other non-chlorinated solvents, which could have different non-covalent interactions with the network (for example hydrogen bonding or π-π stacking) should also be tested in the future. $[ZnCu(CN)_4]_n^{n-}$ unit remains a moiety of interest in terms of its ability to entrap solvents and cations in its large cavities as a novel coordination polymer network.

2.4 EXPERIMENTAL

For all reactions within this thesis, all manipulations were performed in air using purified solvents. The amine ligands ethylenediamine (en), diethylenetriamine (dien), and all other reagents were obtained from commercial sources and used as received.

CAUTION: Although we have experienced no difficulties, perchlorate salts are potentially explosive and should only be used in small quantities and handled with care.

For all complexes within this thesis, IR spectra were obtained using a Thermo Nicolet Nexus 670 FT-IR spectrometer. Microanalyses (C, H, N) were performed at Simon Fraser University by Mr. Miki Yang. Solid-state visible reflectance data were obtained using an Ocean Optics SD2000 spectrometer with reflectance fibre-optics cables and converted into absorbance data. TGA analysis data were obtained using Shimadzu TGA-50 Thermogravimetric Analyzer.

Variable temperature magnetic susceptibility data were collected using a Quantum Design SQUID XL-7 Evercool magnetometer working from 300 to 2 K at field strength of 1 T. Polycrystalline samples were packed into gelatin capsules, which were mounted in low-background diamagnetic plastic straws. When the sample was air- or moisture- sensitive (e.g. **3.2** in chapter 3), a custom-made, air-tight sample holder made of poly(vinylchloride) was used. The sensitive samples were loaded in a glovebox, carried in a Schlenk tube out of the box, brought to the SQUID and rapidly inserted. Final data were corrected for the diamagnetism of the constituent atoms using Pascal constants.[32].

2.4.1 Preparation of $[Cu(en)_2][Zn(NC)_4(CuCN)_2]$ (2.1)

To a 15 ml aqueous solution of $Cu(ClO_4)_2 \cdot 6\ H_2O$ (0.037 g, 0.1 mmol) was added a 3 mL aqueous stock solution (0.100 M) of ethylenediamine (en). While

stirring, a 10 ml aqueous solution of $K_2Zn(CN)_4$ (0.025 g, 0.1 mmol) was added to this purple solution. The resulting solution was partially covered and allowed to slowly evaporate for a week. Large, dark purple blocks of $[Cu(en)_2][Zn(NC)_4(CuCN)_2]$ (**2.1**) were collected by vacuum filtration, washed with H_2O, followed by methanol, and left to air-dry. Yield based on copper: 0.009 g (50.7%). Anal. Calcd. For $C_{10}H_{16}N_{10}Cu_3Zn$: C, 22.56; H, 3.03; N, 26.31. Found: C, 22.81; H, 3.10; N, 26.48. IR (KBr, cm^{-1}): 3333(m), 3283(m), 2136(m), 2128(vs), 2111(vs), 2089(m), 2082(m), 2067(m), 1573(m), 1383(w), 1275(w), 1161(w), 1091(m), 1042(vs), 973(w), 685(m), 530(m), 473(w), 460(w), 443(w). Solid-state visible absorbance: λ_{max} = 541 nm. μ_{eff} (300 K) = 1.8 μ_B.

2.4.2 Preparation of $[Cu(en)_2]_{0.5}[CuZn(NC)_4][C_6H_5Cl]_n$ (2.2)

To a 15 ml aqueous solution of $Cu(ClO_4)_2 \cdot 6\ H_2O$ (0.037 g, 0.1 mmol) was added a 3 mL aqueous stock solution (0.100 M) of ethylenediamine (en). While stirring, a 10 ml aqueous solution of $K_2Zn(CN)_4$ (0.025 g, 0.1 mmol) was added to this purple solution. Then 10 mL chlorobenzene was added to the aqueous solution and the mixture was stirred for 10 minutes. The resulting solution was partially covered and allowed to slowly evaporate for a week. Large, blue hexagon shaped blocks of $[Cu(en)_2]_{0.5}[CuZn(NC)_4][C_6H_5Cl]_n$ (**2.2**) were collected by vacuum filtration, washed with H_2O, and left to air-dry. Yield based on copper: 0.006 g (30.6%). The formula of 2.2 with an unknown number of solvents is based on IR and X-ray data, but does not perfectly match the elemental analysis result. Anal. Calcd. For $[Cu(en)_2]_{0.5}[CuZn(NC)_4][C_6H_5Cl]$: C, 32.95; H, 3.00; N, 19.21. For $[Cu(en)_2]_{0.5}[CuZn(NC)_4][C_6H_5Cl]_{0.5}$: C, 28.36; H, 2.78; N 22.05, Found:

C, 26.29; H, 3.49; N, 23.48. IR (KBr, cm^{-1}): 3333(m), 3276(m), 2956(w), 2893(w), 2116(vs), 1586(m), 1477(m, PhenCl), 1280(w), 1086(w), 1036(s), 1006(s), 963(m), 743(s, PhenCl), 702(m, PhenCl), 685(m), 468(s, PhenCl).

2.4.3 Preparation of $[Cu(en)_2]_{0.5}[CuZn(NC)_4][ClC_2H_4Cl]_n$ (2.2a)

To a 15 ml aqueous solution of $Cu(ClO_4)_2 \cdot 6\ H_2O$ (0.037 g, 0.1 mmol) was added a 3 mL aqueous stock solution (0.100 M) of ethylenediamine (en). While stirring, a 10 mL aqueous solution of $K_2Zn(CN)_4$ (0.025 g, 0.1 mmol) was added to this purple solution. Then 10 mL dichloroethane was added to the aqueous solution and the mixture was stirred for 10 minutes. The resulting solution was partially covered and allowed to slowly evaporate for a week. Large, blue hexagon shaped blocks of $[Cu(en)_2]_{0.5}[CuZn(NC)_4][ClC_2H_4Cl]_n$ (**2.2a**) were collected by vacuum filtration, washed with H_2O, and left to air-dry. Yield based on copper: 0.008 g (39.7%). The formula of 2.2a with unknown number of solvents is based on IR and X-ray data, but not matching the elemental analysis result. Anal. Calcd. For $[Cu(en)_2]_{0.5}[CuZn(NC)_4][ClC_2H_4Cl]$: C, 22.67; H, 2.85; N, 19.83. For $[Cu(en)_2]_{0.5}[CuZn(NC)_4][ClC_2H_4Cl]_{0.5}$ C, 22.46; H, 2.69; N, 22.45. Found: C, 22.18; H, 3.33; N, 20.84. IR (KBr, cm^{-1}): 3341(m), 3282(m), 2963(w), 2896(w), 2119(vs), 1584(m), 1462(m), 1282(m), 1238(m), 1091(m), 1034(s), 970(m), 877(w), 701(m), 447(m).

2.4.4 Preparation of $[Cu(en)_2]_{0.5}[CuZn(NC)_4](CHCl_3)$ (2.3)

To a 15 ml aqueous solution of $Cu(ClO_4)_2 \cdot 6\ H_2O$ (0.037 g, 0.1 mmol) was added a 3 mL aqueous stock solution (0.100 M) of ethylenediamine (en). While

stirring, a 10 ml aqueous solution of $K_2Zn(CN)_4$ (0.025 g, 0.1 mmol) was added to this purple solution. Then 10 mL chloroform was added to the aqueous solution and the mixture was stirred for 10 minutes. The resulting solution was partially covered and allowed to slowly evaporate for a week. Large, red blocks of $[Cu(en)_2]_{0.5}[CuZn(NC)_4](CHCl_3)$ (**2.3**) were collected by vacuum filtration, washed with H_2O, and left to air-dry. Yield based on copper: 0.007 g (23.6%). Anal. Calcd. For $C_7H_9N_6Cu_{1.5}ZnCl_3$: C, 18.92; H, 2.04; N, 18.91. Found: C, 19.26; H, 2.29; N, 19.08. IR (KBr, cm^{-1}): 3473 (w), 3323 (m), 3269 (m), 3217 (w), 3114 (w), 3023 (w), 2999 (w), 2959 (w), 2896 (w), 2152 (s), 2125 (vs), 2112 (vs), 1580 (m), 1571 (m), 1567 (m), 1466 (m), 1462 (m), 1281(m), 1213 (w), 1159 (w), 1092 (m), 1037 (s), 972 (m), 880 (w), 768 (vs, $CHCl_3$), 754(vs, $CHCl_3$), 684 (m), 670 (m, $CHCl_3$), 532 (m), 457 (m), 418 (s).

2.4.5 Preparation of $[Ni(en)_2][Ni(CN)_4]$-2.16H_2O (2.4)
Trans- $[Ni(en)_2][Ni(CN)_4]$-2.16H_2O (2.4.1)
Cis- $[Ni(en)_2][Ni(CN)_4]$-2.16H_2O (2.4.2)[3]

To a 15 ml methanol solution of $Ni(NO_3)_2 \cdot 6\ H_2O$ (0.029 g, 0.1 mmol) was added a 6 mL aqueous stock solution (0.100 M) of ethylenediamine (en). While stirring, a 30 ml methanol solution of $K_2Zn(CN)_4$ (0.050 g, 0.2 mmol) was added to this green solution. The resulting solution was partially covered and allowed to slowly evaporate for 3 days. Dark purple blocks of $[Ni(en)_2][Ni(CN)_4]$-2.16H_2O (**2.4**) were collected by vacuum filtration, washed with H_2O, and left to air-dry. Two types of purples crystals with different size were collected and later identified by single crystal X-ray diffraction as trans-$[Ni(en)_2][Ni(CN)_4]$-2.16H_2O

[3] Thanks to Alex Au, who did this synthesis when he was a Chem481 student under my supervision.

(small) **(2.4.1)**, and cis-$[Ni(en)_2]$- $[Ni(CN)_4]$-2.16H_2O (large) **(2.4.2)**[30] IR (KBr, cm^{-1}): **Trans (2.4.1):** 2158 (s), 2147 (vs), 2134 (vs), 2117 (s); IR (KBr, cm^{-1}): **Cis (2.4.2)**: 2115 (s), 2141 (s).

2.4.6 Preparation of $[Ni(dien)Ni(CN)_4]_n$-$(H_2O)_n$ (2.5)

To a 15 ml methanol solution of $Ni(NO_3)_2 \cdot 6\ H_2O$ (0.029 g, 0.1 mmol) was added a 4 mL aqueous stock solution (0.100 M) of diethylenetriamine (dien). While stirring, a 30 ml methanol solution of $K_2Zn(CN)_4$ (0.050 g, 0.2 mmol) was added to this green solution. The resulting solution was partially covered and allowed to slowly evaporate for a week. Round, flat purple crystals of $[Ni(dien)Ni(CN)_4]_n$-$(H_2O)_n$ **(2.5)** were collected by vacuum filtration, washed with H_2O, and left to air-dry. The crystal structure was reported by Inaki Muga in 2004.[31] IR (KBr, cm^{-1}): 2170 (s), 2159 (s), 2132 (s).

CHAPTER 3: CYANOMETALLATE -BASED POLYMERS WITH GAS STORAGE PROPERTIES

3.1 INTRODUCTION

During recent years, due to the compelling demand for a substitute for fossil-fuel technology, strong attention has been drawn to the field of fuel cell technology, which is so far the most promising substitute.[33] The issue of hydrogen storage and the appropriate materials remains as one of the most challenging problems for fuel cell technology to be applied in the transportation sector. The current target set by the U.S. Department of Energy (DOE) has been made with the concept that today's vehicles will be powered by the future's higher efficiency fuel-cell technology. Thus, the 2010 energy density targets for a hydrogen storage system are 6.0 wt% and 45 kg H_2 per m^3, including the container and necessary components (wt% is defined as the weight of adsorbed gas divided by the weight of adsorbent). The 2015 goal is even more demanding: 9.0 wt% and 81 kg H_2 per m^3.[34] To put this into perspective, the density of elemental hydrogen is only 70.8 kg per m^3 in its liquid state at 20 K (1 atm).

Although two of the currently most developed technologies, compressed hydrogen gas and cryogenically stored liquid hydrogen, can meet the technical goal of the DOE 2010 target, they are unlikely to comply with the 2015 one.[35] In both cases, the container and other components which maintain the necessary high pressure and low temperature contributes at least 90% to the system mass. Also, a large amount of energy is wasted in the process of condensation.

Understandably, new storage materials with higher hydrogen affinity and milder operational conditions have been considered the most possible way of a breakthrough. Solid metal hydrides have been studied for years, especially for the mechanism of hydrogen adsorption at interstitial sites.[36] For example, the theoretical hydrogen uptake has been calculated to be 150 kg H_2 per m^3 for Mg_2NiH_4.[37] Although the amount of hydrogen uptake is very promising (7% the highest), metal hydrides do experience problems of high cost, susceptibility to impurities, low reversibility and high mechanical process requirements.

To circumvent some of these issues, highly porous materials like activated carbon have been investigated for their ability to physisorb molecular hydrogen. Although some successes have been achieved for carbon nano-tube materials, with uptakes of 5 wt% at 77 K,[38] theoretical modeling of the interaction of carbon and hydrogen shows that only a few wt% is the limit for this type of material.[39]

Coordination polymers have been studied for decades with respect to their versatile crystal structures and interesting physical properties.[40] Although it has only been a few years since the first reported coordination polymer with permanent porosity, many recent studies have been done about the structural and functional aspects of coordination polymers.[41] To date, nearly 5000 2D and 3D coordination polymer structures have been reported in the literature, but only a fraction of them have been tested for their gas-storage capacity (especially hydrogen). Compared to conventional porous materials that are being widely studied, such as zeolites and activated carbon, coordination polymers have the intrinsic advantages of ease of synthesis and functionalization of their organic

linkers, and their highly crystalline nature, which guarantees the reproducibility and consistency of physical properties.[42]

Coordination polymers are assembled by the connection of metal ions or clusters through molecular bridges. All porous coordination polymers to date are microporous (pore size less than 2 nm) and have a type I isotherm (see below).[43] The most outstanding relevant property of coordination polymers is their large apparent surface area, which makes them interesting candidates for H_2 storage.[44] The highest wt% achieved at 77 K/1 atm so far for coordination polymers is approximately 2.5 wt%.[45] Recently, the hydrogen adsorption capacity data for a series of known Prussian Blue analogue compounds was reported.[9] By removing H_2O (bonded or non-bonded) from the crystal lattice and metal centres in the array, nano-sized pores and coordinatively unsaturated metal sites were generated in the dehydrated solid, which has about a 1-2 wt% hydrogen adsorption capacity at LN_2 temperature and 1 atm.[9] The surface area data was also measured for such materials by an N_2 adsorption test. Since some of our previously synthesised coordination polymers showed vapochromic properties,[46] which suggested possible porous behaviour, we prepared a new type of tetrahedral-based cyanometallate network, along with two octahedral cyanometallate-based networks. Their synthesis and porosity and ability to adsorb hydrogen gas is described in this chapter, after a short tutorial on gas adsorption measurements.

3.1.1 Theory of Surface Area and Porosity Analysis

A relatively great proportion of the atoms of a fine powder are near the surface. This causes powders to show distinctly different physical properties from their bulk form. Many of the properties are strongly related to the magnitude of their surface area and porosity. Usually a fine powder is more reactive than its bulk form and has more adsorptive capacity. In some instances the surface area and morphology is even more influential than the chemical composition.[47]

Gas adsorption is the most commonly used characterization technique for determination of the specific surface area, pore volume, and pore size distribution as well as to study the surface properties.[47] Since gas adsorption is a complex phenomenon involving mass and energy interaction, many theories have been proposed for the description of this complicated process.[47] Some of the theories are appropriate under specific conditions and others are applicable in wider circumstances. In order to investigate the pore structure of a powder, an adsorption (or desorption) isotherm must be established first. This is a measure of the molar quantity of gas taken up (or released) by the powder as a function of gas pressure, at a constant temperature.[48] Generally, the physical adsorption of gases by solids increases with decreased temperature and with increased pressure. The adsorption process is exothermic. The test is most frequently carried out at cryogenic temperature, usually the boiling point of liquid nitrogen (LN_2) – 77.35K at one atmosphere pressure. Conventionally, the quantity of gas is expressed as its volume at standard conditions of temperature and pressure (STP, 273.15 K and 760 torr) and the pressure is expressed as a relative

pressure, which is the actual gas pressure P divided by the vapour pressure P_o of the gas at the experiment temperature. In a hydrogen adsorption test, the weight percentage of H_2 is more frequently used for comparison purposes, which does not change the shape of the isotherm.[49]

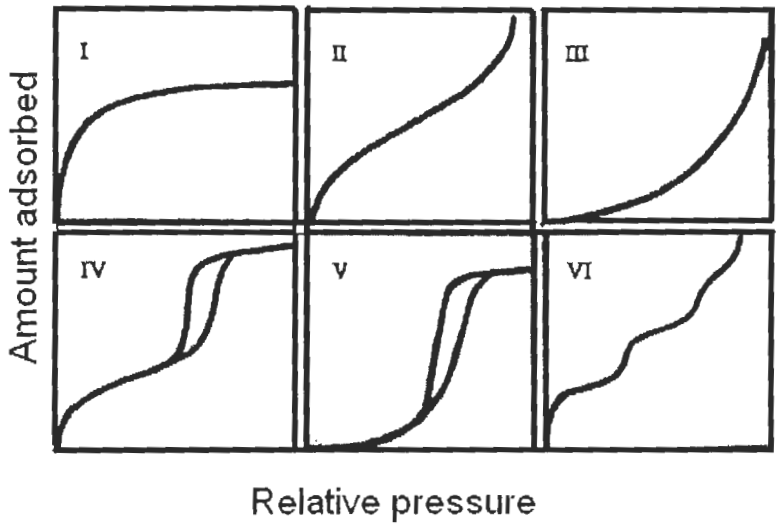

Figure 3-1: IUPAC adsorption isotherms I to VI.[50]

Adsorption isotherms generally follow one of six forms (Figure 3-1), each of which reveals much about the structure of the absorbing material. Types one and two are the types that are most frequently seen in the tests of organic-inorganic coordination polymer materials. Type one is characteristic of adsorbents having extremely small pores with strong adsorbent-adsorbate interaction. Types two and four are indicative of either nonporous adsorbents or adsorbents with relatively large pores, where the isotherm curve rises comparatively rapidly at low relative pressure, rises moderately at intermediate relative pressure, and then rapidly at the saturation pressure. Types three and

five isotherms are for materials where their affinity with adsorptive molecules is weaker than the affinity of the molecules with each other and an acceleration adsorption effect can be observed from the isotherm curve. The isotherm of type six is quite rare, and it's indicative of a nonporous solid with completely uniform surface. By testing the same material with different gases, different types of isotherm can be generated. So "large" and "small" pore size are all relative terms depending on which testing gas is being used. Some types of nonporous (type two isotherm) powder for N_2 can be porous (type one) for H_2.

Conventionally, pores are classified on the basis of their diameter as micropores (below 2 nm), mesopores (between 2 and 50 nm), and macropores (above 50 nm). Considering that the span of the linear building block –M-C-N-M'- has a length about only 0.6 nm, most cyanometallate coordination polymers, if they are porous at all, fall under the category of micropores.[51]

Compared to materials with bigger pore sizes, microporous materials have an extraordinary adsorption capacity.[50] The isotherm curve almost rises vertically at very low pressure, and levels off to a long and nearly horizontal section. This indicates that the pores fill up very quickly and then very little adsorption takes place after the micropores have been filled. This is not a surface phenomenon but rather is enhanced adsorption in micropores under a driving force of quite low relative pressure. It should be noted that the curve for a type I isotherm in Figure 3-1 is for a hypothetical completely microporous material with a very narrow range of pore size distribution, whereas actual materials can have pores in all size ranges, and the isotherm shape may vary enormously.

In order to extract information from the measured isotherm, many adsorption theories have been developed. All the theories are applicable only for specific type of materials under certain testing conditions. Below, several widely accepted theories are introduced.

Langmuir Isotherm

The Langmuir theory is more applicable to chemisorption situations than to physical adsorption ones.[52] It assumes that gases form only one molecular layer on a solid. Collision of a gas molecule with the solid surface is assumed to be inelastic, and a gas molecule remains on the solid surface for a time before returning to the gas phase. This time delay is taken as the cause for the phenomenon of adsorption. The model, described by equation (1), considers monolayer adsorption in which adsorption at all sites is equivalent and independent of adsorption at neighbouring sites.

$$V_a = \frac{V_m bP}{1 + bP} \qquad \text{(Equation 1)}$$

In equation 1, V_m is a constant representing the limiting adsorption capacity and b is a constant exponentially related to the positive value of the adsorption energy.

For the hydrogen uptake isotherm of a microporous solid (type two or four), the Langmuir model is mostly suitable. Because of the relatively poor affinity between H_2 and the solid surface, usually only a part of the surface area can be

occupied, first the most energetic regions and then the less energetic regions. Under normal experimental conditions, like 77 K/1 atm, no more than one layer of H_2 can be formed and that fulfils the basic assumption of the Langmuir model.[52]

Langmuir-Freundlich Isotherm

This model,[53] described by equation (2), is a combination of the Langmuir model with the Freundlich equation, which allows a logarithmic fall in the enthalpy of adsorption with surface coverage as the most energetic area will be occupied first; it gets harder for adsorption to occur when only the less energetic regions are left.

$$V_a = \frac{V_m b P^{(1/t)}}{1 + bP^{(1/t)}} \qquad \text{(Equation 2)}$$

In equation 2, V_m is a constant representing the limiting adsorption capacity, b is a constant exponentially related to the positive value of the adsorption energy and t is a constant related to the fall-off in adsorption enthalpy. Compared to the more commonly used Langmuir equation, the Langmuir-Freundlich equation gives an accurate fit over a larger pressure range.

BET Theory:

The Brunauer-Emmett-Teller (BET) model is one of the major methods to evaluate specific surface area from adsorption isotherms.[54] The BET theory generalized Langmuir's model and incorporated the concept of multimolecular layer adsorption. The fundamental assumptions are: the surface is flat; all adsorption sites have the same adsorption energy; the adsorption energy for all molecules except those of the first layer is equal to the liquefaction energy; and an infinite number of layers can form.

$$V_a = \frac{V_m C P}{(P_0 - P)\left[1 + (C-1)\frac{P}{P_0}\right]} \qquad \text{(Equation 3)}$$

C in equation 3 is a constant that is related to the heat of adsorption of the first layer and is a different value from sample to sample, P_0 is the saturation pressure of the gas, and V_m is a constant representing the limiting adsorption capacity.

Equation 3 can also be written in the linear form shown in equation 4.

$$\frac{P}{V_a (P_0 - P)} = \frac{1}{V_m C} + \frac{(C-1)}{V_m C}\frac{P}{P_0} \qquad \text{(Equation 4)}$$

from which, if applicable, a plot of $P/[V_a(P_o-P)]$ *vs.* P/P_o should yield a straight line with intercept $1/V_mC$ and slope $(C\text{-}1)/V_mC$. Usually C is a very big

number and the intercept can be approximated as insignificant. This is equivalent to assuming that $1/V_mC=0$ and $(C\text{-}1)/V_mC=1/V_m$ where V_m can be easily calculated from the slope directly. The specific surface area of the adsorbent, the area of 1 gram of it, is then calculated from V_m by

$$S=V_mN_A\sigma/mV_0 \qquad \text{(Equation 5)}$$

Where $\boldsymbol{\sigma}$ is the area of surface occupied by a single adsorbed gas molecule (16.2 $Å^2$ in the case of nitrogen), N_A the Avogadro constant, m the mass of adsorbing sample, and V_0 the molar volume of the gas (22414 cm^3). This equation may vary in form when the V_m is represented in units other than cm^3.

In general, it is recommended to use adsorption data at relative pressures between 0.05 and 0.3 in N_2 BET calculations, where the plot of eq. 4 is linear. Between those pressure-ranges, the first N_2 layer is being completed and more molecules are stacking on top of the first layer to form the second one, where the assumptions of BET model are most closely fulfilled.[55] Type one isotherms are generally analyzed by the BET model. For hydrogen adsorption isotherms, the BET model is rarely applied because only a small fraction of the solid surface is covered by H_2 and the experimental pressure is far below the lower limit of 0.05 P_0 of Hydrogen.

3.1.2 Custom-Made Porosity Apparatus

A custom-made porosity instrument (constructed by Professor Ian Gay) applying a static volumetric method was used for measuring isotherm data in this thesis. Each data point on the adsorption isotherm is measured individually and manually using mass balance equations, gas equations of state and measured pressures. The static volumetric system basically consists of a gas manifold joined to a sample holder by an isolation valve. Onto the manifold part are connected a pressure transducer and inlets from the adsorptive gas reservoirs. To start the test, first a certain amount of gas is released from a gas reservoir to a manifold with a measurable volume V_1 and pressure P_1. (Figure 3-2) The initial gas quantity is calculated by the universal gas law $n_1=P_1V_1/RT$. Then the manifold is connected to the vacuumed sample holder containing a dried solid sample. After waiting for a few minutes for the adsorption to reach its equilibrium, the volume V_2 and pressure P_2 can be measured again, and remaining gas quantity can be calculated the same way as $n_2=P_2V_2/RT$. Then the gas quantity absorbed by the solid sample is simply $n=n_1-n_2$.

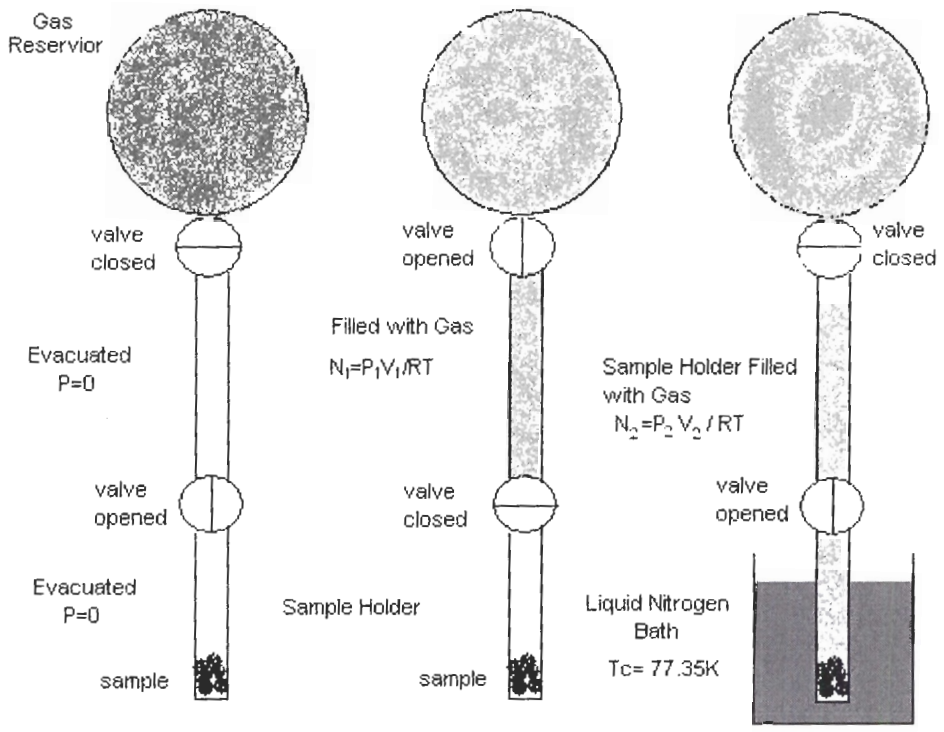

Figure 3-2: Schematic diagram of gas adsorption measurement sequence in a static volumetric, low temperature system.

It's worth noting that since the sample holder is partially immersed in LN_2 at about 77 K, there are two different temperature zones (77 K and room temperature) for the total volume, and a steep temperature gradient between the two zones. So when measuring the remaining gas quantity n_2, the volume V_2 is not the actual volume of sample holder plus the manifold, but a pre-calibrated volume as if the temperature was a constant over the total volume. Helium gas is used in this free space measurement, because it is not absorbed in discernible quantities by most samples and it behaves as an ideal gas.

Thus, to obtain V_2, the sample holder and manifold are first evacuated, the isolation valve is closed, and the manifold is charged with helium to pressure P_1. Then the isolation valve is opened, helium enters the sample holder at LN_2 temperature and the pressure becomes P_2. Since helium is not absorbed by the solid sample, the gas quantity is constant throughout the test. A helium-calibrated sample holder volume then can be calculated as $V_2=P_1V_1/P_2$ (assuming the temperature is RT over the manifold and sample holder). V_2 can be used in future calculations for adsorptive gas tests as long as the volume of the sample holder immersed in LN_2 is kept the same throughout the tests.

After the adsorption isotherm is generated by measuring the data point by point, more information such as surface area and adsorption enthalpy (two isotherms at different temperature are needed) can be analysed and extracted from the isotherm by fitting it to different adsorption models.

3.2 RESULTS AND ANALYSES of $CoZn(CN)_4$

3.2.1 Synthesis and Characterization of $CoZn(CN)_4 \cdot 4H_2O$ and $CoZn(CN)_4$

The reaction of an aqueous solution of 1 equivalent of $Co(NO_3)_2 \cdot 2H_2O$ with an aqueous solution of 1 equivalent of $K_2Zn(CN)_4$ produced an immediate orange precipitate of $CoZn(CN)_4 \cdot 4H_2O$ **(3.1)** in 90% yield. The orange precipitate was filtered, washed with H_2O and dried in air. When vacuum or heat (120 °C) was applied to the orange solid, the colour of **3.1** changed from orange to blue within 30 minutes. Elemental analysis confirmed the blue compound was the dehydrated $CoZn(CN)_4$ **(3.2)**, which is extremely hydroscopic. When exposed to

moisture, it can reabsorb H_2O in the solid state to form the orange **3.1** in one minute (Figure 3-3).

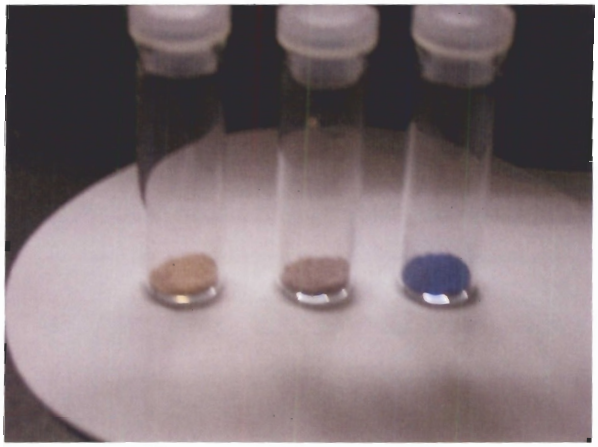

Figure 3-3: Orange $CoZn(CN)_4 \cdot 4H_2O$ (left); Purple partially dehydrated sample (Middle); Blue $CoZn(CN)_4$ (right).

The TGA of **3.1** (Figure 3-4) shows only one weight loss step from room temperature to 100 °C, consistent with the loss of four H_2O (24% calculated, 25% observed). The dehydrated blue **3.2** was stable until 350 °C, at which point it decomposed via loss of cyanogen and the metal residues reacted with oxygen, forming a mixture of Co_2O_3 (or Co_3O_4, quite hard to differentiate from the TGA diagram) and ZnO mixture (final weight percentage, 53% calculated, 49% observed, This discrepancy may be due to drift, visible from 100 °C to 350 °C).

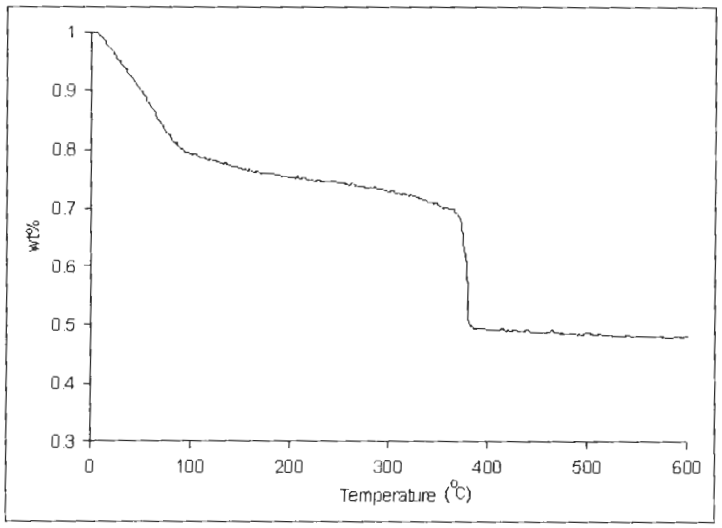

Figure 3-4: TGA analysis of 3.1 from room temperature to 600 °C.

Variable temperature IR spectroscopy was also carried out from RT to 200 °C (Figure 3-5). Below 80°C, there is one major cyanide peak of **3.1** at 2177 cm^{-1} and a smaller one at 2214 cm^{-1}. When heated up to 100 °C, another peak at 2195 cm^{-1} starts to emerge and gains higher intensity at higher temperature. The peak at 2177 cm^{-1} also shows a gradual red-shift to 2169 cm^{-1} and the small peak at 2214 cm^{-1} disappears with elevated temperature. The data suggests the cyanide binding environment is changed after a structure transformation. Since all of the peaks are blue-shifted from the original $K_2Zn(CN)_4$ peak at 2155 cm^{-1}, Co-CN-Zn (or Zn-CN-Co) bridging or even triply-bridged cyanides may exist in the structures of both **3.1** and **3.2**. The fact that both compounds have multiple νCN stretches implies that their structures do not correspond to the previously reported simple diamond 3D network in the stoichiometrically related adamantane-like $[NMe_4][ZnCu(CN)_4]$, since it has only one cyanide peak at 2135 cm^{-1} and all four cyanides are structurally equivalent.[56]

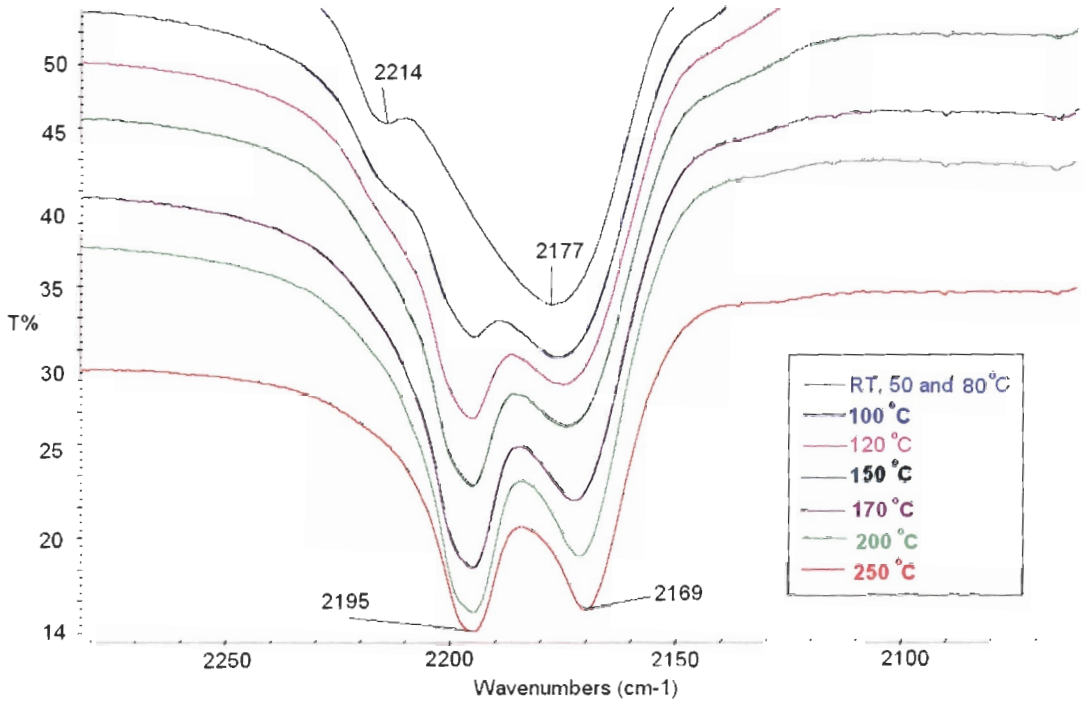

Figure 3-5: Variable temperature IR spectra for 3.1 from RT to 250 °C, focusing on the vCN region from 2000 to 2300 cm^{-1}.

Variable temperature magnetic susceptibility measurements (from 300 to 1.8 K) of **3.1**(upper) and **3.2** (lower) are depicted in Figure 3-6. The μ_{eff} for **3.1** at 300 K is only 2.89 μ_B, and upon dehydration, **3.2** exhibits a reduced μ_{eff} of 2.58 μ_B per Co^{2+} ion. Although the Co^{2+} ion in **3.1** is most likely octahedrally coordinated and in **3.2** tetrahedrally coordinated because of their distinctive colours, both the μ_{eff} values are far below the range typically found for tetrahedrally coordinated Co^{2+} ions(3.98 to 4.82 μ_B) and for octahedrally coordinated Co^{2+} ions(4.77 to 5.40 μ_B).[57] This suggests antiferromagnetic coupling between Co^{2+} ions, mediated by superexchange through the possible bridging water molecules or cyanides. The sharpened decline in $\chi_M T$ at lower temperature, however, could most likely due to

a combination of zero-field splitting and unquenched orbital angular momentum of the Co^{2+} ion.

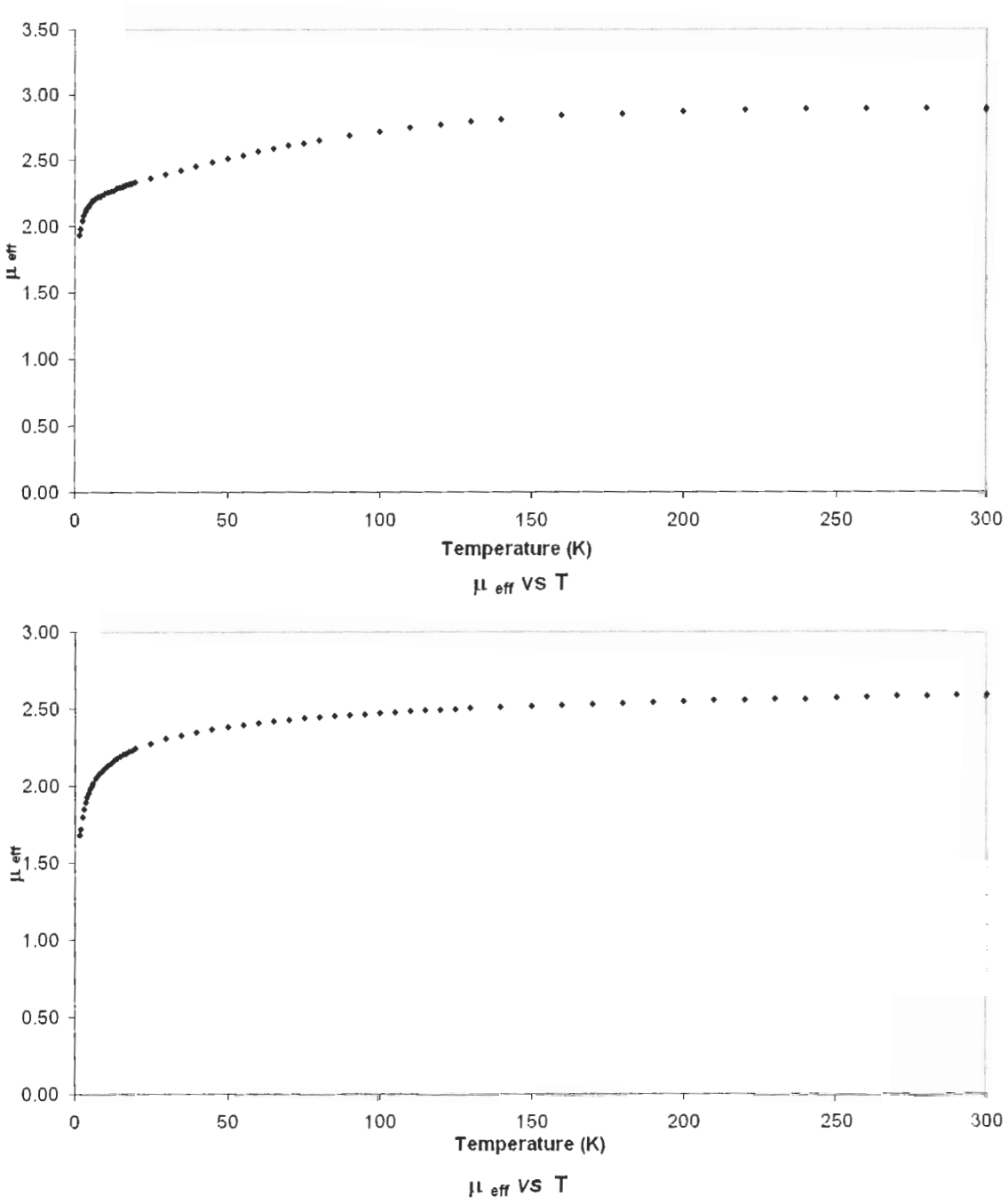

Figure 3-6: Temperature dependence of μ_{eff} for 3.1 (top) and 3.2 (bottom).

Several methods to obtain single crystals of **3.1** were attempted, including H-tube and Hydrothermal methods. However, due to the lability of $[Zn(CN)_4]^{2-}$, all of the slow diffusion methods generated other compounds (mostly bright purple or pink solids with cyanide IR peaks), but not **3.1**, in the form of powders. The powder X-ray diffraction pattern (baseline flattened to account for a very broad background bump throughout the whole spectra, possibly caused by the sample holder) of **3.1** is shown in Figure 3-7. This diffractogram can be indexed to two sets of unit cells (Hexagonal/trigonal, a=b=8.3349 Å, c= 7.2442 Å, α=β=90°, γ=120°; Tetragonal: a=b=7.2288 Å, c= 15.2970 Å, α=β=γ=90°). The quality of the crystalline powder of **3.1** is not very good, due to the fast precipitation process by which it is prepared. It is worth noting that the hydration-dehydration reaction between **3.1** and **3.2** is completely reversible. The compound re-hydrated from **3.2** exhibits the same IR, powder XRD and magnetic susceptibility data as freshly prepared **3.1**. For compound **3.2**, the powder X-ray diffraction experiment had a high background and no observable peaks, indicating its low crystalline or even amorphous nature.

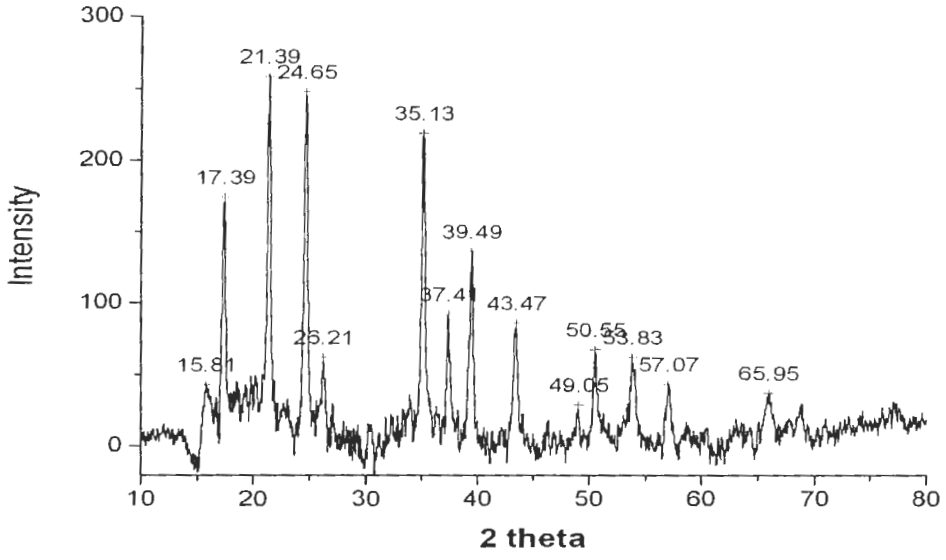

Figure 3-7: X-ray powder diffraction pattern for 3.1.

3.2.2 Gas Adsorption Properties of $CoZn(CN)_4$

Recent literature has illustrated that microporous structures can be generated by dehydrating Prussian Blue analogues.[9] By removing both coordinated and uncoordinated water from $M^{II}_3[Co^{III}(CN)_6]_2 \cdot xH_2O$, an open cubic framework with vacancies and channels is formed and it exhibits a hydrogen affinity of 1-2 wt% at 77K/1atm.

In light of these results, the porosity of the dehydrated $CoZn(CN)_4$ sample was probed via a nitrogen adsorption measurement performed at LN_2 temperature (77 K). Solid **3.1** was first completely dehydrated to yield **3.2** by heating at 100 °C for 48 hours under dynamic vacuum. It's worth noting that dehydration at a higher temperature resulted in a lower gas adsorption capacity, presumably as a result of partial framework collapse. The nitrogen sorption

isotherm for **3.2**, shown in Figure 3-8, is typical for a microporous material in which a monolayer of nitrogen is formed at very low relative pressures.

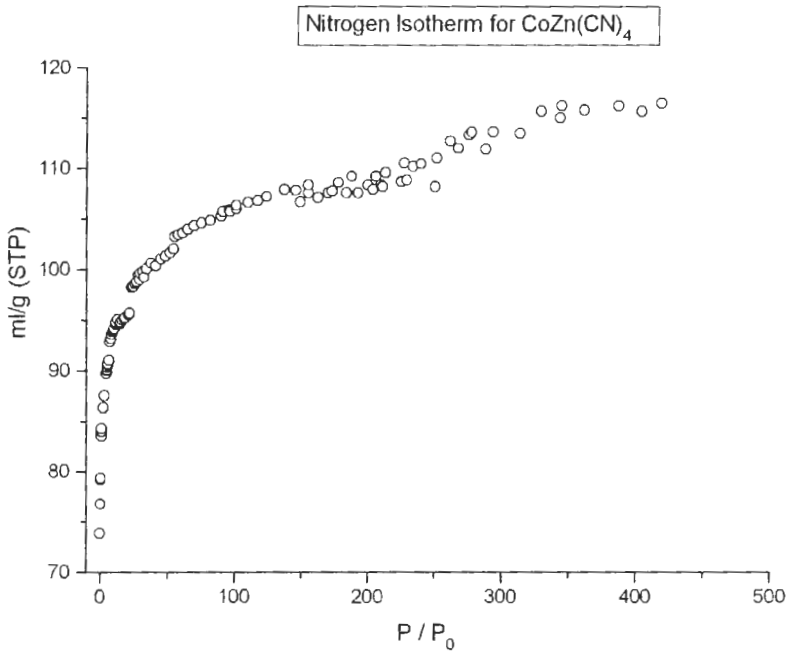

Figure 3-8: Nitrogen sorption isotherm for CoZn(CN)4 (3.2) at 77 K.

The surface area is calculated by applying the BET model to the data. The plot of $P/[V_a(P_o-P)]$ *vs.* P/P_o yielded a straight line between P/P_o from about 0.01 to 0.2 (Figure 3-9) . A surface area of 399 m^2/g is calculated from V_m, which is determined by the intercept $1/V_mC$ and slope $(C-1)/V_mC$ (calculation method is detailed in the introduction of BET model in section 3.1.1).

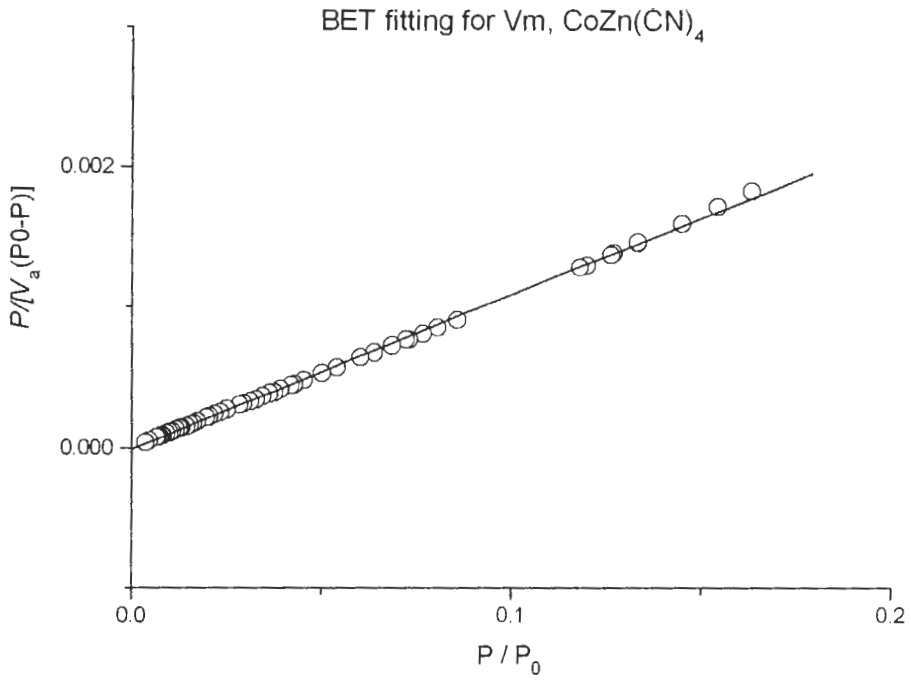

Figure 3-9: Rearranged BET fitting for $CoZn(CN)_4$. Plot of $P/[V_a(P_o-P)]$ *vs.* P/P_o.

Using the same volumetric apparatus, the hydrogen sorption isotherm was also collected at 77 K (Figure 3-10). The isotherm data was fitted by the Langmuir- Freundlich equation, shown in the graph as a solid line. Extrapolation of the fit gives a prediction of 0.77 wt% at 1 atm and 1.3 wt. % H_2 adsorbed at infinite pressure.

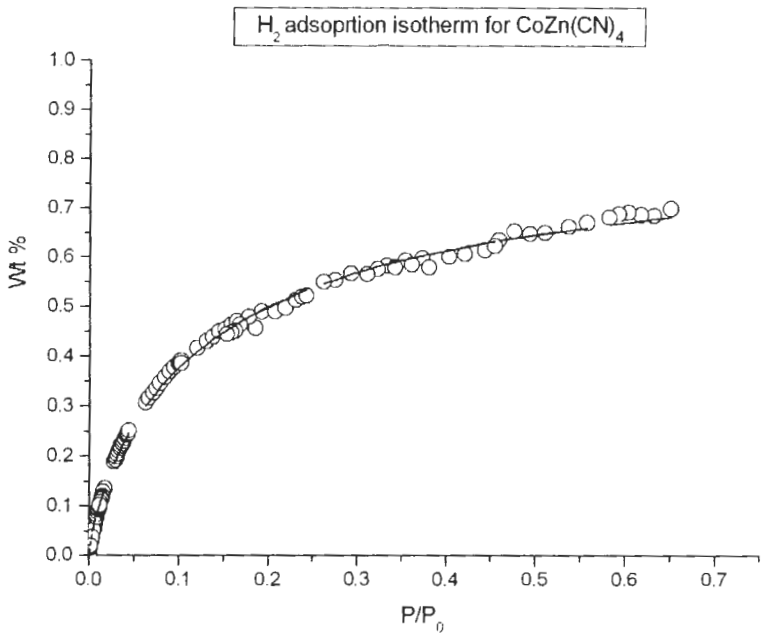

Figure 3-10: Hydrogen adsorption isotherm for $CnZn(CN)_4$ (3.2) at 77 K

Although relatively small, the surface area and the hydrogen adsorption capacity of **3.2** are still consistent with previously reported porous coordination polymers (not only cyanide-based), which exhibited surface areas from 300 to 4526 m^2/g and H_2 uptake at 1 atm from 0.2 to 2.5 wt%.[41] It also proves that there is no linear relationship between the surface area and H_2 uptake, since the surface area is tested and calculated from nitrogen isotherm, and H_2 and N_2 have very different features for storage materials. For example, compound **3.2** achieved 0.77 wt% H_2 uptake at 77 K/ 1 atm with a relatively small surface area at 399 m^2/g, in comparison to the coordination polymer with largest surface area reported (4526 m^2/g) and its 1.61% H_2 uptake at the same condition.[58] Although surface area is a very important parameter for gas-storage-material, a large surface area does not necessarily guarantee a high H_2 adsorption capacity.

Compounds with large surface areas (i.e. can absorb a large quantity of N_2) can also exhibit a relatively small H_2 uptake at the same time. The more important corollary is that it is not necessary to have a very large surface area (by N_2 adsorption) to potentially have significant H_2 adsorption capacity.

Solid **3.1** was also tested and shows no porosity toward both N_2 and H_2 at 77 K.

3.2.3 Other Endeavours with the $[Zn(CN)_4]^{2-}$ Building Block

Due to the lability of $[Zn(CN)_4]^{2-}$, many of the reactions performed with $[Zn(CN)_4]^{2-}$ and other first row transition metal ions (Mn^{2+}, $Fe^{3+/2+}$, Ni^{2+}, Cu^{2+}) resulted in impure products that could not be characterized conclusively. For example, when $Fe(NO_3)_3 \cdot 9H_2O$ was reacted with $Zn(CN)_4^{2-}$ in aqueous solution, a green mixture precipitated which had multiple cyanide stretchings in the IR spectrum. In order to explore this issue of Zn-CN lability, the reaction between Zn^{2+} and $K_3Fe(CN)_6$ was attempted to see if the same compound or mixture would be produced. A yellow precipitate (which is different from the reaction between Fe^{3+} and $K_2Zn(CN)_4$) was formed immediately upon mixing of the two reagents, and could further transform to yet another complex by heating in air. Although no $[Zn(CN)_4]^{2-}$ containing compounds were synthesized using $[Fe(CN)_6]^{3-}$ as a starting material, another Zn-containing bimetallic coordination polymer, of the Prussian Blue family was discovered which also exhibits gas storage capacity, as discussed in the next section.

3.3 RESULTS AND ANALYSES of $KZn[Fe(CN)_6]$ and $KCd[Fe(CN)_6]$

3.3.1 Synthesis and Characterization of $KM[Fe(CN)_6]\cdot nH_2O$ (M = Zn, Cd)

The reaction of an aqueous solution of 1 equivalent of $M(NO_3)_2$-nH_2O (M=Cd, Zn, n=4, 6) with an aqueous solution of 1 equivalent of $K_3Fe(CN)_6$ produced an immediate yellow precipitate of $KM[Fe(CN)_6]\bullet nH_2O$ (**3.3**: M= Cd, n=4.2; **3.4**: M=Zn, n=7).The yellow precipitate was centrifuged, filtered, washed with H_2O and dried in air. Compounds **3.3** and **3.4** are not stable under room temperature and in air. They slowly lose water and transform to $KM[Fe(CN)_6]\cdot nH_2O$ (**3.5**: M=Cd, n=2.2 ; **3.6**: M=Zn, n=2) with apparent colour changes from yellow to greenish blue, which is stable in air. When vacuum and heat (120 °C) are further applied to **3.5** or **3.6**, all the water molecules can be removed, and the colours of both compounds remain the same. Elemental analysis confirmed the resulting compounds were dehydrated $KM[Fe(CN)_6]$ (M= Cd,Zn) (**3.7** and **3.8**). The dehydrated compounds (**3.7** and **3.8**) can quickly absorb H_2O to form the air-stable compounds **3.5** and **3.6** when they are exposed to moisture, while the greenish blue colour remains similar (Figure 3-11).

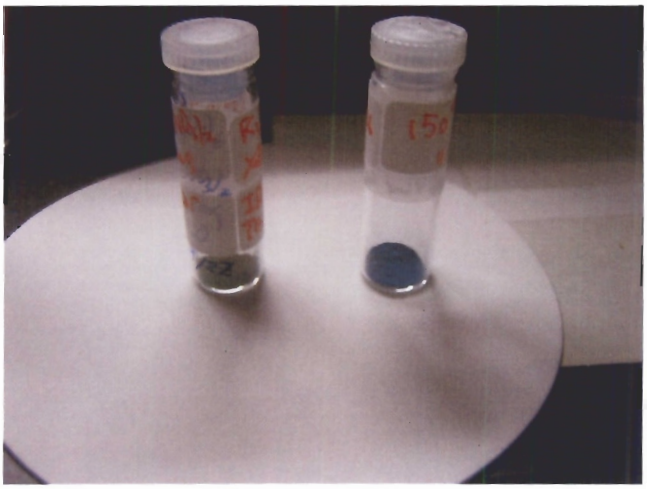

Figure 3-11: Yellow $KCd[Fe(CN)_6]\cdot 4.2H_2O$ (3.3, left); Green $KCd[Fe(CN)_6]$ (3.7, right).

The TGA data for **3.4** (Figure 3-12) shows two step weight losses. The first step, below approximately 120 °C, corresponds to the loss of seven water molecules (calculated 29%, observed 27%). The second step between 250 and 350 °C tracks the decomposition of $KZn[Fe(CN)_6]$ into K_2O, ZnO and Fe_2O_3 (final weight 46% calculated, 43% observed). The TGA data for **3.3** and **3.4** are very similar.

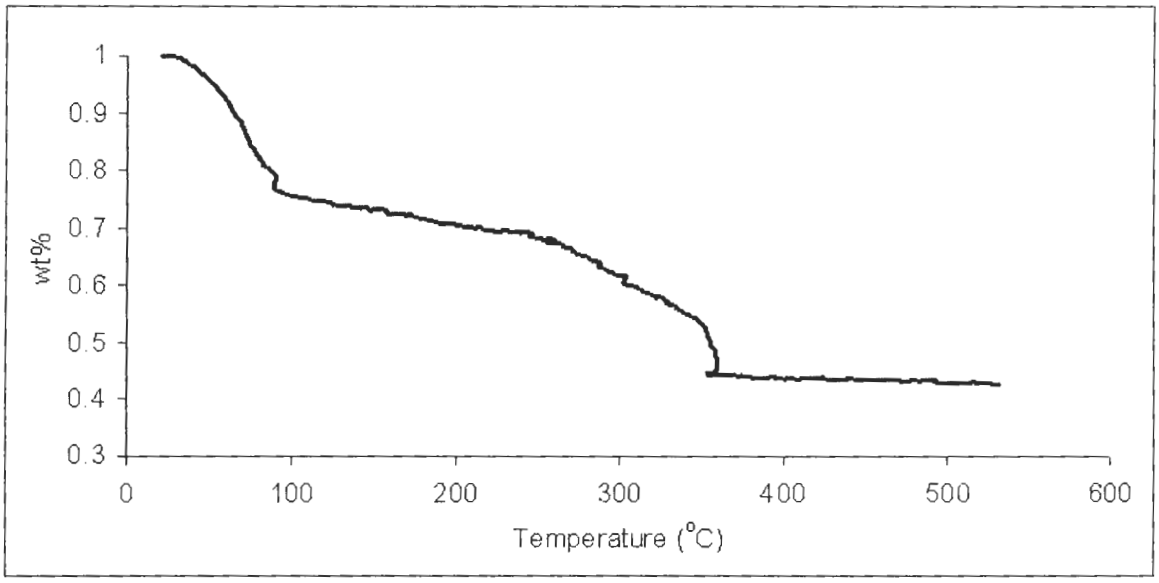

Figure 3-12: TGA analysis for 3.4 from room temperature to 550 °C.

For the as-synthesized hydrated compounds, there are two major cyanide peaks at 2135 cm^{-1} and 2063 cm^{-1} for **3.3** (2164 cm^{-1} and 2096 $cm^{-1}$for **3.4**) which shows that there are at least two types of inequivalent cyanides existing in the structure. The partially dehydrated compounds **3.5** and **3.6** only show one cyanide peak, at 2161 cm^{-1} for **3.5** (2092 cm^{-1} for **3.6**). That is a clear sign of structure transformation. On the other hand, **3.7** and **3.**8 have the same cyanide peaks for **3.5** and **3.6**, indicating the structures remain the same upon further dehydration.

The powder X-ray diffraction pattern of partially dehydrated compound **3.5** is shown in Figure 3-13. Although the high angle peaks are quite weak, the major peaks below 40 degree in 2θ can be indexed to a cubic cell with a= 10.58 Å. Thus, the partially dehydrated compound **3.5** likely has a Prussian Blue-type cubic structure. Considering the chemical formulas of both compounds have a

K:Fe:Zn ratio of 1:1:1, the most possible structure is the type III structure (Figure 3-14) with half the cubic cavities being occupied by potassium ions. **3.6** is isostructural to **3.5**, having a cubic cell with a=10.14 Å (Ionic Radius: Zn^{2+}, 0.74 Å; Cd^{2+}, 0.97 Å).

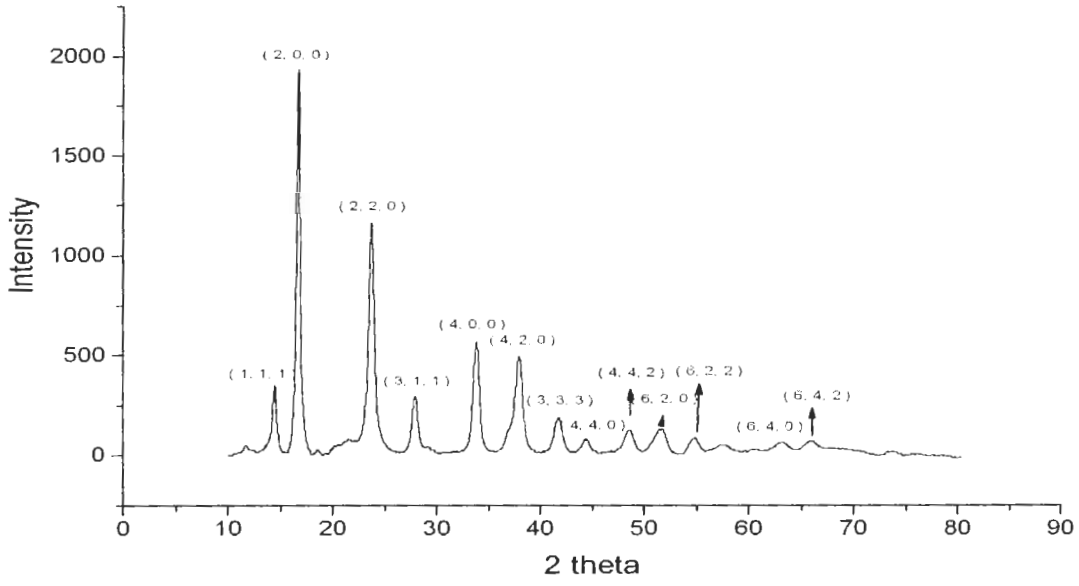

Figure 3-13: X-ray powder diffraction pattern for 3.5. Indexed to a cubic cell, a=10.58 Å.

Depending on the oxidation state of the metal ions, more than one type of cavity can be generated from the basic type II PB structure in Figure 3-14, where all the metal ions are 3+ and the cubic network itself $Fe(III)Fe(III)(CN)_6$ is neutral. If one equivalent of Fe^{3+} ion is replaced by M^{2+} (for example Zn^{2+}) and the ratio of Fe^{3+} and M^{2+} is 4:4, the cubic network is not reduced and being anionic, another four equivalents of K^+ (or Na^+) will be introduced into the structure, occupying half of the tetrahedral sites in order to balance the charges. Thus, **3.5** and **3.6** are both type III PB structure where K:Fe(III):Zn(II)=1:1:1.

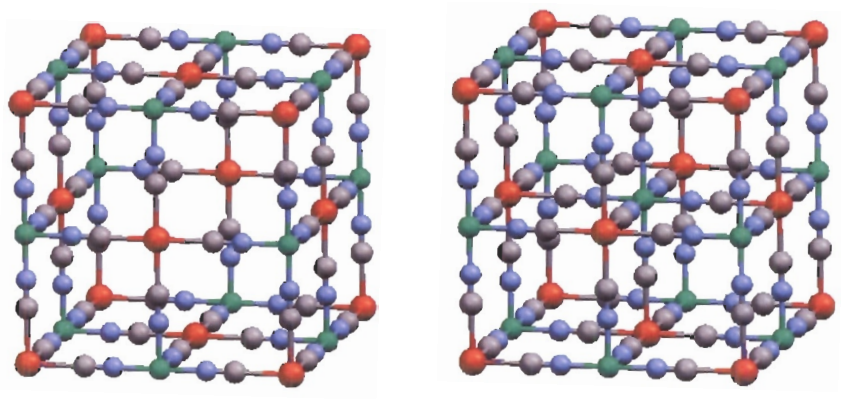

Type I: $Fe_4[Fe(CN)_6]_3$ **Type II: $Fe[Fe(CN)_6]$**

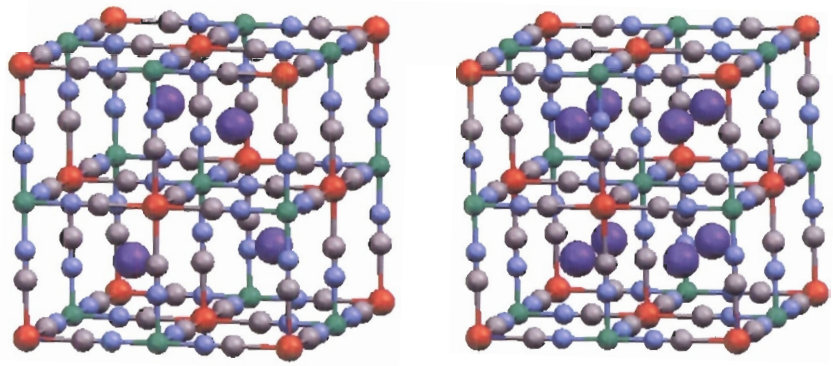

Type III: $KM[Fe(CN)_6]$ **Type IV: $K_2M[Fe(CN)_6]$**

Figure 3-14: Four general types of Prussian Blue structure.[59]

3.3.2 Gas Adsorption Properties of $KM[Fe(CN)_6]$ (M = Zn, Cd)

Although all of the cubic channels are blocked by the potassium ions, the dehydrated compounds still exhibit porosity with respect to nitrogen and hydrogen gas. The same measurement technique as described for **3.2** was utilized for **3.7** and **3.8** (dehydration was completed before gas adsorption tests, and it's confirmed by Elemental Analysis). It's quite surprising that both **3.7** and

3.8 are porous to nitrogen, because there is almost not enough space around the potassium ions left for N_2 to penetrate into the pores.

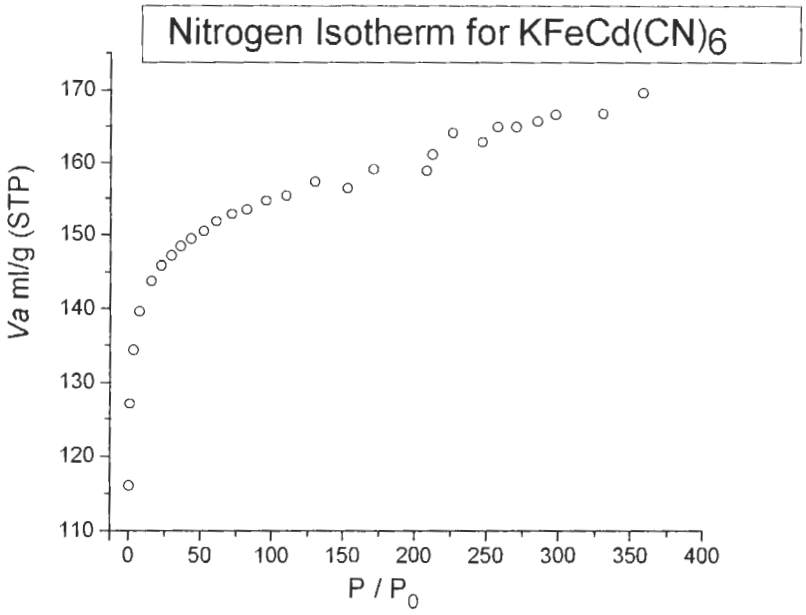

Figure 3-15 : Nitrogen sorption isotherm for $KCd[Fe(CN)_6]$.

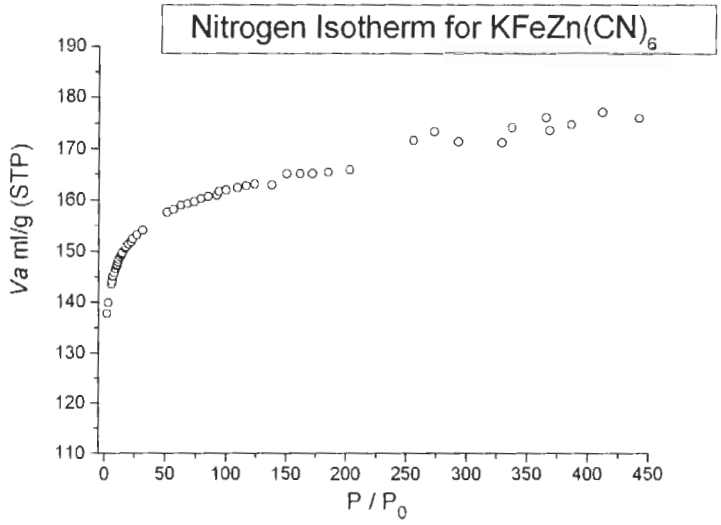

Figure 3-16: Nitrogen sorption isotherm for $KZn[Fe(CN)_6]$.

The surface area was calculated by applying the BET model to the data. The plot of $P/[V_a(P_o-P)]$ *vs.* P/P_o yielded a straight line between P/P_o from about 0.01 to 0.2 (Figure 3-17 and Figure 3-18). A surface area of 580 m^2/g for **3.7** and 615 m^2/g for **3.8** is calculated from V_m, which is determined by the intercept $1/V_mC$ and slope $(C-1)/V_mC$.

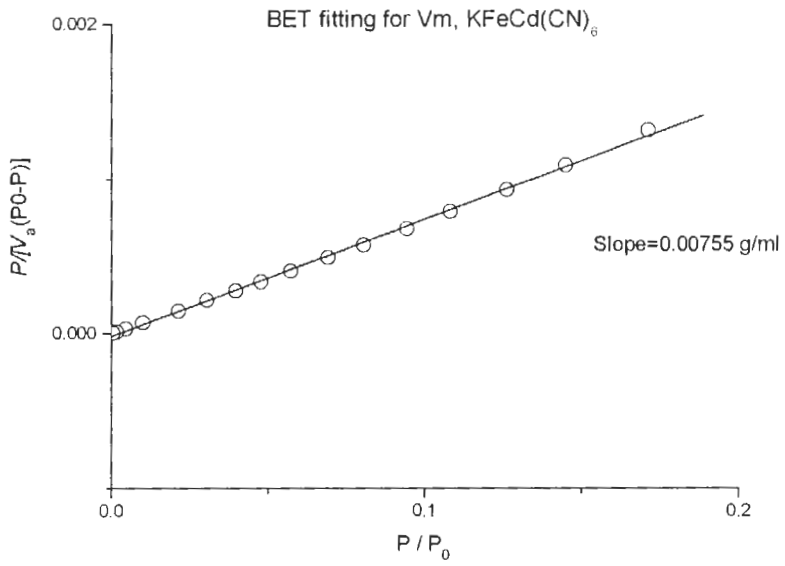

Figure 3-17: Rearranged BET fitting for KCd[Fe(CN)$_6$]. Plot of $P/[V_a(P_o-P)]$ *vs.* P/P_o.

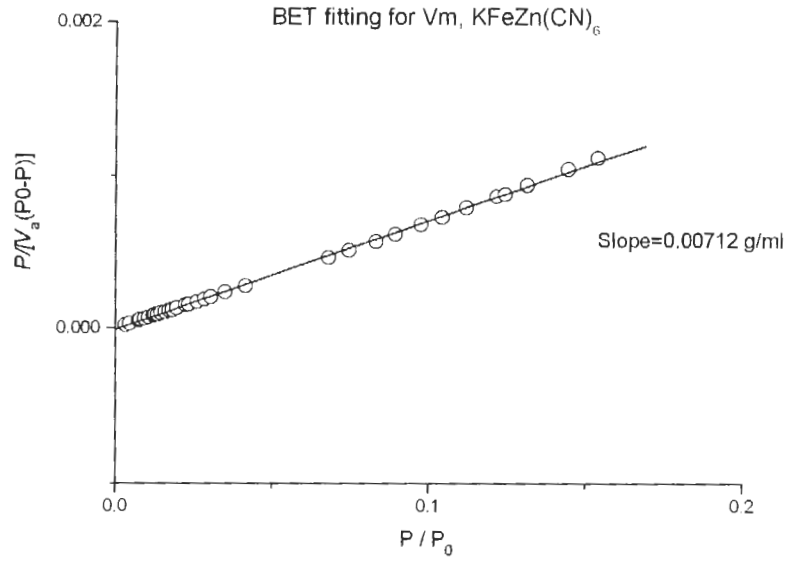

Figure 3-18: Rearranged BET fitting for KZn[Fe(CN)$_6$]. Plot of $P/[V_a(P_o-P)]$ *vs.* P/P_o.

Using the same volumetric apparatus, Hydrogen sorption isotherms were collected at 77 K for **3.5** and **3.6**. (Figure 3-19 and Figure 3-20). The isotherm data was fitted by the Langmuir- Freundlich equation, which is shown in the graph as a solid line. Extrapolation of the fit gives a prediction of 0.93 wt% at 1 atm and 1.74 wt% H_2 adsorbed at infinite pressure for **3.5**, and 1.01 wt% at 1 atm and 1.41 wt% at infinite pressure for **3.6**.

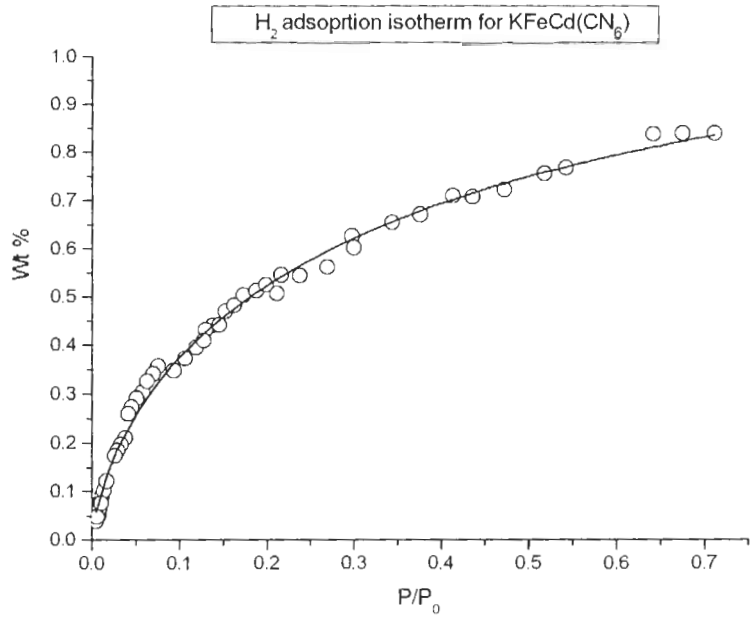

Figure 3-19: Hydrogen sorption isotherm for $KCd[Fe(CN)_6]$.

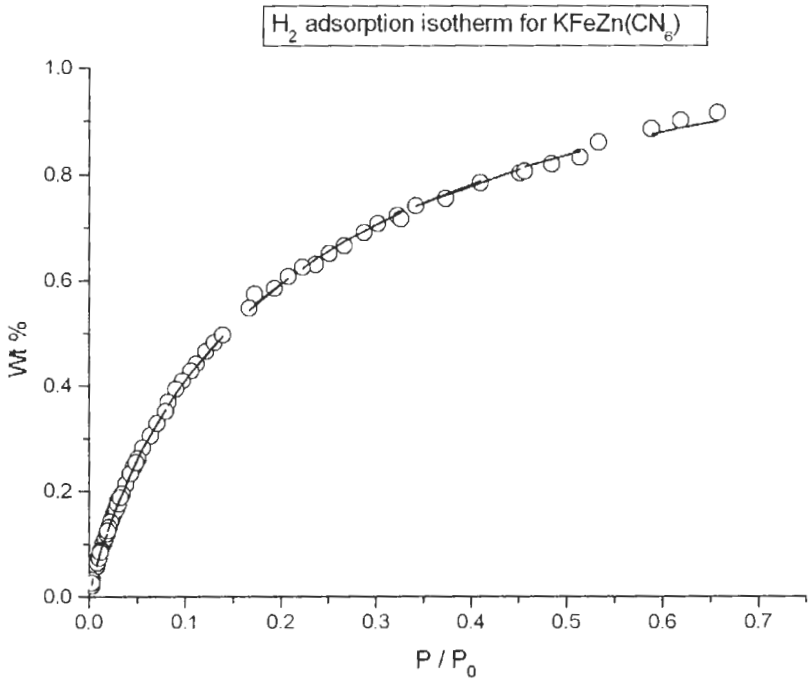

Figure 3-20: Hydrogen sorption isotherm for $KZn[Fe(CN)_6]$.

Comparing to the previously-tested $[Co(CN)_6]^{3-}$-containing Prussian Blue analogues (Table 3-1), the gas adsorption capacities of **3.7** and **3.8** are about 60% to 70% of the $[Co(CN)_6]^{3-}$ PB compounds (excluding $Ni_3[Co(CN)_6]_2$, whose surface area is unexpectedly small compared to other type I PBs) for both N_2 and H_2 adsorptions.[9] This suggests that a large empty space and unused surface metal charges are not the only dominating factors in gas adsorption. Considering the fact that, in the type III PB structure, half of the eight tetrahedral sites are occupied by large potassium ions, and all the transition metals are saturated (six coordinated), the adsorption results for type III PB reported here should be considered to be better than expected, given the free volume decrease that would have intuitively been predicted for type III vs. type I. It is possible that the potassium ion, despite its space-occupying and channel-blocking character, is also playing some positive roles in the gas adsorption process. After all, the physisorption process is driven by the van der Waals interaction between the surface and the gas, and it is very possible that K^+, with its 18 electrons, is part of the "surface" and does attract a few gas molecules by itself. Although most porous material research is still focusing on the synthesis of materials with larger empty spaces, bigger channels and energetic spots (e.g. unsaturated metal sites), putting something into the big pores (instead of large unused space) could be equally important.[58] A large empty room is not that useful unless there is some furniture.

A test of the gas adsorption capacity for type IV Prussian Blue $K_2MM'(CN)_6$ should be helpful to understand this issue.

Table 3-1: Comparison of type I and type III Prussian Blue material's gas adsorption data.

	Surface Area (m^2/g)	Wt % H_2 (77K)
$Mn_3[Co(CN)_6]_2$ [9]	870	1.6 [a]
$Fe_3[Co(CN)_6]_2$ [9]	770	1.4 [a]
$Co_3[Co(CN)_6]_2$ [9]	800	1.5 [a]
$Ni_3[Co(CN)_6]_2$ [9]	560	1.4 [a]
$Cu_3[Co(CN)_6]_2$ [9]	730	1.8 [a]
$Zn_3[Co(CN)_6]_2$ [9]	720	1.4 [a]
$KCdFe(CN)_6$	580	0.97 [a], 0.93 [b]
$KZnFe(CN)_6$	615	1.05 [a], 1.01 [b]
$ZnCo(CN)_4$ [c]	399	0.80 [a], 0.77 [b]

[a] data at 890 torr; [b] data at 760 torr; [c] Structure Unknown

3.4 CONCLUSIONS AND FUTURE WORKS

It has been illustrated that porous coordination polymers have been generated by removing the solvent (water) molecules from the structure. Sometimes the main framework remains intact and sometimes a structural change is involved in the process. Reversible colour changes have been demonstrated by incorporating Co^{2+} and the $[Zn(CN)_4^{2-}]$ building block together,

although structural details are still unknown and need to be worked out. It's quite likely that the dehydrated $CoZn(CN)_4$ shows vapochromic properties with other organic solvents, and it should be tested as well.

It also showed that type III PB materials with their seemingly blocked (no open channel) structures can still exhibit substantial surface area and H_2 uptake capacity. The potential positive effect of the potassium ions in the PB type III structure remains a subject of interest if analogous compounds with other alkali metals with smaller atomic mass can be synthesised, for example $LiKFe(CN)_6$, which could possibly improve the overall gravimetric gas adsorption rate by lower the molar mass of absorbent. Other types of Prussian Blue materials, e.g. type I like $Fe_4[Zn(CN)_6]_3$, type II, or even type IV like $K_2FeZn(CN)_6$, are certainly interesting area to explore too, since apparently they possess void space with different sizes in their structures than type III, and comparisons between those may further elucidate the mechanism of adsorption for microporous materials.

3.5 EXPERIMENTAL

General experimental is the same as described in section 2.4. Gas porosity measurement is described in section 3.1.2. Before adsorption, the samples (about 100 mg) were dehydrated at temperatures at 383 K for 12 hours under vacuum. The adsorption was measured in the partial pressure range 0.0 to 0.7, referenced to atmospheric pressure.

3.5.1 Preparation of $CoZn(CN)_4 \cdot 4H_2O$ (3.1)

To a 25 mL aqueous solution of $Co(NO_3)_2$-$6H_2O$ (145 mg, 0.50 mmol) was added a 15 mL aqueous solution of $K_2Zn(CN)_4$ (127 mg, 0.50 mmol). An immediate orange precipitate was formed, which was filtered, washed with 15 mL of water three times, and air-dried overnight. Yield: 135 mg (90%). Anal. Calcd. for $CoZnC_4N_4H_8O_4$: C, 15.99; H, 2.68; N, 18.65. Found: C, 15.89; H, 2.48; N, 18.41. IR (KBr): 3440 (s), 2178 (s), 2143 (w), 1612 (m), 1384 (w), 445 (s) cm^{-1}.

3.5.2 Preparation of $CoZn(CN)_4$ (3.2)

Solid $CoZn(CN)_4 \cdot 4H_2O$ (**3.1**) was heated to 100 °C under vacuum. The orange powder changed colour to blue after 12 hours. The blue solid of $CoZn(CN)_4$ (**3.2**) was hydroscopic at room temperature and needed to be kept in dry and sealed vials. Yield: 100%. Anal. Calcd. for $CoZnC_4N_4$: C, 21.03; H, 0; N, 24.50. Found: C, 21.11; H, 0; N, 24.20. IR (KBr, 200 °C): 2195 (s), 2169 (s), 1612 (vw, small amount of H_2O, possibly from the KBr pellet); 1384 (vw, H_2O), cm^{-1}.

3.5.3 Preparation of $KFeCd(CN)_6 \cdot 4.2H_2O$ (3.3)

To a 40 mL aqueous solution of $Cd(NO_3)_2 \cdot 4H_2O$ (616 mg, 2.0 mmol) was added a 40 mL aqueous solution of $K_3Fe(CN)_6$ (658 mg, 2.0 mmol). An immediate yellow precipitate was formed, which was centrifuged, filtered, then washed with 25 mL of water three times, and air-dried overnight. Yield: 360 mg (41%). Anal. Calcd. for $KFeCdC_6N_6(H_2O)_{4.2}$: C, 16.41; H, 1.93; N, 19.13. Found: C, 16.26; H, 1.95; N, 19.11. IR (KBr): 3498 (m), 2135 (s), 2063 (s), 1611 (m), 1384 (vw), 593 (w), 512 (w), 413 (m) cm^{-1}.

3.5.4 Preparation of $KFeZn(CN)_6 \cdot 7H_2O$ (3.4)

To a 20 mL aqueous solution of $Zn(NO_3)_2 \cdot 6H_2O$ (315 mg, 1.0 mmol) was added a 20 mL aqueous solution of $K_3Fe(CN)_6$ (329 mg, 1.0 mmol). An immediate yellowish orange precipitate was formed, which was centrifuged, filtered , then washed with 15 mL of water three times, and air-dried overnight. Yield: 320 mg (72.3%). Anal. Calcd. for $KFeZnC_6N_6(H_2O)_7$: C, 16.28; H, 3.19; N, 18.99. Found: C, 16.56; H, 3.02; N, 18.68. IR (KBr): 3654 (s), 3440 (s), 2164 (s), 2096 (s), 1611 (s), 1384 (w), 993 (w), 603 (w), 494 (w), 427 (w) cm^{-1}.

3.5.5 Preparation of $KFeCd(CN)_6 \cdot 2.2H_2O$ (3.5)

1g of solid yellow **3.3** was placed on a petri-dish in air for a week. The solid changed colour to greenish-blue, to form $KFeCd(CN)_6 \cdot 2.2H_2O$ (**3.5**). Yield: 100%. Anal. Calcd. for $KFeCdC_6N_6O_{2.2}H_{4.4}$: C, 17.88; H, 1.10; N, 20.85. Found: C, 18.01; H, 0.72; N, 20.41. IR (KBr): 3456 (m), 2063 (vs), 1613 (m), 592 (m), 470 (m) cm^{-1}.

3.5.6 Preparation of $KFeZn(CN)_6 \cdot 2H_2O$ (3.6)

1g of solid yellow **3.4** solid was placed on a petri-dish in air for a week. The solid changed colour to greenish-blue, to form $KFeZn(CN)_6 \cdot 2H_2O$ (**3.6**). Yield: 100%. Anal. Calcd. for $KFeZnC_6N_6O_2H_4$: C, 20.45; H, 1.14; N, 23.84. Found: C, 20.30; H, 1.01; N, 23.48. IR (KBr): 3466(m), 2095(vs), 1613(m), 600(m), 496(m) cm^{-1}.

3.5.7 Preparation of $KCd[Fe(CN)_6]$ (3.7)

Yellow $KCd[Fe(CN)_6]\cdot 4.2H_2O$ (**3.3**) was heated in air at 150 °C (or under vacuum at 100 °C). The yellow solid changed colour to green after 20 minutes to yield the hygroscopic solid $KCd[Fe(CN)_6]$ (**3.7**). Yield: 100%. Anal. Calcd. for $KFeCdC_6N_6$: C, 19.83; H, 0; N, 23.12. Found: C, 19.96; H, 0.02; N, 22.82. IR (KBr, 200 °C): 3456 (vw), 2061 (s), 1613 (vw), 590 (m), 468 (w) cm^{-1}.

3.5.8 Preparation of $KZn[Fe(CN)_6]$ (3.8)

Yellow $KZn[Fe(CN)_6]\cdot 7H_2O$ (**3.4**) was heated in air at 150 °C (or under vacuum at 100 °C). The yellow solid changed colour to blue after 20 minutes, to yield the hygroscopic solid of $KZn[Fe(CN)_6]$ (**3.8**). Yield: 100%. Anal. Calcd. for $KFeZnC_6N_6$: C, 22.77; H, 0; N, 26.56. Found: C, 22.62; H, 0.04; N, 26.20. IR (KBr, 200 °C): 3477(vw), 2092(s), 1613(vw), 598(w), 491(w) cm^{-1}.

APPENDIX 1: SUMMARY OF CRYSTALLOGRAPHIC DATA

Data for all crystal structures described throughout this thesis were collected for each single crystal (mounted on a glass fiber) at room temperature, using the diffractometer control program DIFRAC[60] and an Enraf Nonius CAD4F diffractometer. The programs used for all absorption corrections; data reduction and all structure solutions contained within this thesis were from the *NRCVAX* Crystal Structure System[61]. The structures were refined using CRYSTALS[62]. Diagrams were made using Mercury[63].

The following pages contain summary tables of the crystallographic data and refinement details for all reported structures contained in this thesis. The complete list of fractional atomic coordinates and equivalent isotropic thermal parameters (U(iso) in $Å^2$) are collected in Appendix 2.

Table 1: Summary of Crystallographic Data.

	2.1	2.2 (a)	2.2(b)	2.3
Formula	$C_{10}H_{16}Cu_3N_{10}Zn_1$	$C_{0.67}Cu_{0.17}N_{0.67}O_{0.17}Zn_{0.17}$	$C_{4.50}Cl_{0.50}Cu_{1.76}N_{11.50}Zn_2$	$C_{12.48}Cl_{7.39}Cu_{2.62}N_{10.48}Zn_2$
Formula Weight	532.32	41.50	475.38	855.76
Crystal Habit	Purple Block	Blue Prism	Blue Prism	Red Block
Crystal Dimensions (mm^3)	0.20 x 0.29 x 0.43	0.25 x 0.31 x 0.70	0.23 x 0.32 x 0.40	0.27 x 0.27 x 0.45
Space Group	P -1	P 6_3 m c	A m m 2	P 1 2_1 1
a, A	8.5686(18)	8.340(3)	13.2816(17)	8.3532(8)
b, A	10.1532(18)	8.340(3)	25.023(3)	10.8192(12)
c, A	10.9605(18)	13.234(3)	14.451(2)	16.7089(19)
α, deg	88.276(15)	90	90	90
β, deg	84.002(16)	90	90	91.274(8)
γ, deg	68.053(15)	120	90	90
Volume, A^3	879.6(3)	797.2(3)	4802.7(11)	1509.7(3)
Z	2	12	8	2
Calc. density, g/cm^3	2.010	1.037	1.310	1.882
Linear Absorption	49.89	28.09	35.72	40.60
Data range	$4° \le 2\theta \le 60°$	$5° \le 2\theta \le 76°$	$4° \le 2\theta \le 64°$	$4° \le 2\theta \le 56°$
Final Unit Cell Reflections: Range	32: $45° \le 2\theta \le 47°$	49: $35° \le 2\theta \le 37°$	42: $45° \le 2\theta \le 51°$	64: $36° \le 2\theta \le 42°$
Parameters/Observed Data	224/3244	20/1363	108/2411	170/2288
R, R_w (I>2.5 σ(I))	0.039, 0.045	0.247, 0.184	0.100, 0.140	0.133, 0.146

APPENDIX 2: FRACTIONAL ATOMIC COORDINATES

Table 2 : Fractional Atomic Coordinates and Equivalent Isotropic Thermal Parameters (U(iso) in $Å^2$) for $[Cu(en)_2][Zn(NC)_4(CuCN)_2]$ (2.1).

Atom	x	y	z	$U_{iso/equiv}$	Occupancy
Zn1	0.29561(6)	0.41582(5)	0.76458(4)	0.0244	1.0000
Cu1	0.0000	0.0000	-0.5000	0.0319	1.0000
Cu2	0.0000	0.0000	0.0000	0.0328	1.0000
Cu3	0.53226(7)	0.15737(7)	0.16293(5)	0.0331	1.0000
Cu4	0.33397(7)	0.32504(6)	0.31947(5)	0.0285	1.0000
N1	0.0687(5)	0.1671(4)	-0.4964(4)	0.0352	1.0000
N2	-0.2304(5)	0.1443(4)	-0.5234(4)	0.0326	1.0000
N3	0.0808(6)	0.1588(5)	-0.0423(4)	0.0484	1.0000
N4	-0.1951(5)	0.1484(4)	0.0932(4)	0.0387	1.0000
N5	0.4204(5)	0.5459(4)	-0.7656(4)	0.0340	1.0000
N6	0.0487(5)	0.5185(4)	-0.7623(4)	0.0358	1.0000
N7	0.3759(5)	0.2917(4)	-0.9098(3)	0.0327	1.0000
N8	0.3358(5)	0.3283(4)	-0.6026(3)	0.0330	1.0000
N9	0.3357(6)	0.0187(5)	-0.2932(4)	0.0479	1.0000
N10	0.9099(6)	0.0112(5)	-0.2532(5)	0.0524	1.0000
C1	-0.0831(7)	0.2980(5)	-0.4856(5)	0.0426	1.0000
C2	-0.2127(7)	0.2793(5)	-0.5584(5)	0.0417	1.0000
C3	-0.0167(8)	0.2806(6)	0.0398(6)	0.0538	1.0000
C4	-0.1926(8)	0.2891(6)	0.0602(6)	0.0555	1.0000
C5	0.5017(6)	0.6077(5)	-0.7438(4)	0.0304	1.0000
C6	-0.0942(6)	0.5766(5)	-0.7413(4)	0.0303	1.0000
C7	0.4304(6)	0.2338(5)	-1.0015(4)	0.0318	1.0000
C8	0.3467(5)	0.3188(5)	-0.4988(4)	0.0291	1.0000
C9	0.3880(6)	0.0985(5)	-0.2679(4)	0.0330	1.0000
C10	0.7712(6)	0.0642(5)	-0.2138(4)	0.0327	1.0000
H11	-0.0557(7)	0.3762(5)	-0.5159(5)	0.060(9)	1.0000

Atom	x	y	z	$U_{iso/equiv}$	Occupancy
H12	-0.1281(7)	0.3150(5)	-0.4021(5)	0.060(9)	1.0000
H21	-0.1745(7)	0.2759(5)	-0.6432(5)	0.057(9)	1.0000
H22	-0.3181(7)	0.3562(5)	-0.5431(5)	0.057(9)	1.0000
H31	-0.0124(8)	0.3657(6)	0.0039(6)	0.068(10)	1.0000
H32	0.0301(8)	0.2665(6)	0.1161(6)	0.068(10)	1.0000
H41	-0.2524(8)	0.3557(6)	0.1240(6)	0.065(10)	1.0000
H42	-0.2448(8)	0.3191(6)	-0.0135(6)	0.065(10)	1.0000
H51	0.1358(5)	0.1688(4)	-0.5684(4)	0.058(9)	1.0000
H52	0.1297(5)	0.1602(4)	-0.4295(4)	0.058(9)	1.0000
H61	-0.2768(5)	0.1136(4)	-0.5845(4)	0.052(9)	1.0000
H62	-0.3005(5)	0.1572(4)	-0.4504(4)	0.052(9)	1.0000
H71	0.2069(6)	0.1244(5)	-0.0252(4)	0.105(13)	1.0000
H72	0.0746(6)	0.1807(5)	-0.1154(4)	0.105(13)	1.0000
H81	-0.1762(5)	0.1341(4)	0.1875(4)	0.087(13)	1.0000
H82	-0.2843(5)	0.1415(4)	0.0842(4)	0.087(13)	1.0000

Table 3 : Fractional Atomic Coordinates and Equivalent Isotropic Thermal Parameters (U(iso) in $Å^2$) for $[Cu(en)_2][CuZn(NC)_4][C_6H_5Cl]_n$ (2.2a, $P6_3mc$).

Label	x	y	z	$U_{iso/equiv}$	Occupancy
Zn1	0.6667	0.3333	0.5275(4)	0.0479	1.0000
Cu1	0.6667	0.3333	0.9102(5)	0.0550	1.0000
O1	1.0000	0.0000	0.7207(13)	0.0436(18)	1.0000
N1	0.6667	0.3333	0.760(2)	0.076(5)	1.0000
N2	0.5382(6)	0.0764(12)	0.9527(7)	0.0391(17)	1.0000
C1	0.6667	0.3333	0.680(3)	0.099(6)	1.0000
C2	0.5366(14)	0.073(3)	0.4637(16)	0.089(5)	1.0000

Table 4 : Fractional Atomic Coordinates and Equivalent Isotropic Thermal Parameters (U(iso) in $Å^2$) for $[Cu(en)_2][CuZn(NC)_4][C_6H_5Cl]_n$ (2.2b, Amm2).

Label	x	y	z	$U_{iso/equiv}$	Occupancy
Zn1	0.6916(4)	0.3340(3)	0.7983(5)	0.0420	1.0000
Zn2	0.6905(7)	0.5000	0.2956(7)	0.0427	1.0000
Zn4	0.8103(7)	0.5000	0.6298(7)	0.0476	1.0000
Cu1	0.5000	0.0000	0.4623(8)	0.0395	1.0000
Cu3	0.8093(4)	0.1670(3)	0.6315(6)	0.0436	1.0000
Cu5	1.0000	0.1621(7)	0.9490(12)	0.173(5)	1.018(9)
N2	1.103(2)	0.2037(13)	0.882(2)	0.0500	1.0000
N4	1.103(2)	0.1455(13)	1.0595(19)	0.0500	1.0000
N8	0.770(4)	0.228(3)	0.692(4)	0.101(7)	1.0000
N9	0.767(4)	0.103(2)	0.698(3)	0.061(6)	1.0000
N10	0.776(3)	0.4334(19)	0.700(3)	0.053(6)	1.0000
N11	0.758(4)	0.326(2)	1.002(4)	0.110(7)	1.0000
N12	0.773(4)	0.5000	0.499(3)	0.040(6)	1.0000
N13	0.548(2)	0.3378(16)	0.793(3)	0.050(6)	1.0000
N14	0.726(4)	0.5000	0.426(3)	0.039(6)	1.0000
N15	0.548(4)	0.5000	0.280(4)	0.063(6)	1.0000
N16	0.741(3)	0.273(2)	0.729(3)	0.053(6)	1.0000
N17	0.748(2)	0.3354(19)	0.925(2)	0.039(5)	1.0000
N18	0.745(3)	0.0654(19)	0.743(3)	0.039(6)	1.0000
C1	1.199(4)	0.151(3)	1.009(4)	0.141(7)	1.0000
C19	0.744(3)	0.398(2)	0.735(3)	0.039(6)	1.0000
C20	0.965(4)	0.5000	0.616(5)	0.059(7)	1.0000
C21	0.965(2)	0.1692(18)	0.627(2)	0.031(5)	1.0000
C32	1.179(5)	0.202(3)	0.956(4)	0.171(7)	1.0000
Cl8	1.5000	0.1554(18)	0.941(3)	0.213(6)	1.0000

Table 5 : Fractional Atomic Coordinates and Equivalent Isotropic Thermal Parameters (U(iso) in $Å^2$) for $[CuZn(NC)_4][Cu(en)_2(CHCl_3)_2]_{0.5}$ (2.3).

Label	x	y	z	$U_{iso/equiv}$	Occupancy
Zn13	0.7927(5)	0.7042(8)	0.6103(3)	0.0372	1.0000
Zn26	0.2184(5)	1.2172(7)	0.8949(2)	0.0340	1.0000
Cu3	0.7639(9)	1.3483(10)	0.7498(4)	0.0444	0.619(16)
Cu16	0.7023(6)	0.9517(8)	0.3604(3)	0.0488	1.0000
Cu23	0.7203(5)	0.9672(8)	0.8531(3)	0.0389	1.0000
Cl1	0.500(4)	1.575(3)	0.884(2)	0.118(3)	0.64(3)
Cl2	0.504(3)	1.074(3)	0.6176(17)	0.118(3)	0.77(3)
Cl3	0.895(6)	1.466(6)	0.953(3)	0.118(3)	0.38(3)
Cl4	0.717(9)	1.082(8)	0.563(5)	0.118(3)	0.26(3)
Cl33	0.127(4)	1.827(3)	0.8695(18)	0.118(3)	0.64(4)
Cl34	0.383(3)	1.695(3)	0.7944(14)	0.118(3)	0.87(3)
Cl35	0.319(4)	1.643(3)	0.9524(18)	0.118(3)	0.68(4)
Cl36	0.401(3)	0.889(2)	0.5854(14)	0.118(3)	0.89(4)
Cl37	0.239(2)	1.0422(17)	0.6888(10)	0.118(3)	1.19(4)
Cl38	0.088(2)	0.959(2)	0.5505(11)	0.118(3)	1.06(4)
N1	0.504(4)	1.057(4)	0.868(2)	0.052(2)	1.0000
N2	0.271(4)	1.375(4)	0.747(2)	0.052(2)	1.0000
N3	0.248(4)	1.364(4)	1.058(2)	0.052(2)	1.0000
N4	-0.098(4)	1.079(4)	0.861(2)	0.052(2)	1.0000
N5	0.744(4)	0.873(4)	0.751(2)	0.052(2)	1.0000
N6	0.743(4)	0.772(3)	0.505(2)	0.052(2)	1.0000
N7	1.109(4)	0.555(4)	0.631(2)	0.052(2)	1.0000
N8	0.635(4)	0.560(4)	0.631(2)	0.052(2)	1.0000
N31	0.594(3)	1.221(4)	0.699(2)	0.039(5)	0.619(16)
N32	0.900(3)	1.287(4)	0.6504(17)	0.039(5)	0.619(16)
N33	0.888(4)	1.508(3)	0.795(2)	0.039(5)	0.619(16)
N34	0.633(4)	1.379(4)	0.8567(16)	0.039(5)	0.619(16)
C1	0.386(5)	1.097(5)	0.880(3)	0.052(2)	1.0000
C2	0.255(5)	1.345(5)	0.809(3)	0.052(2)	1.0000
C3	0.235(5)	1.295(4)	0.997(3)	0.052(2)	1.0000
C4	0.006(5)	1.157(4)	0.874(3)	0.052(2)	1.0000
C5	0.768(5)	0.833(5)	0.694(3)	0.052(2)	1.0000

Label	x	y	z	$U_{iso/equiv}$	Occupancy
C6	0.734(5)	0.838(5)	0.448(3)	0.052(2)	1.0000
C7	1.007(5)	0.634(4)	0.622(3)	0.052(2)	1.0000
C8	0.495(5)	0.538(4)	0.634(3)	0.052(2)	1.0000
C31	0.676(5)	1.174(4)	0.637(2)	0.039(5)	0.619(16)
C32	0.781(5)	1.248(4)	0.5988(14)	0.039(5)	0.619(16)
C33	0.779(6)	1.554(3)	0.847(2)	0.039(5)	0.619(16)
C34	0.729(6)	1.462(4)	0.8959(15)	0.039(5)	0.619(16)
C39	0.311(6)	1.762(5)	0.875(3)	0.060(13)	1.0000
C40	0.218(6)	0.913(5)	0.617(3)	0.064(13)	1.0000

REFERENCES

[1] a) C. A. Mirkin, B. J. Holliday, *Angew. Chem. Int. Ed.*, **2001**, *40*, 2022. b) L. Ouahab, *Chem. Mater.*, **1997**, *9*, 1909. c) B. Moulton, M. J. Zaworotko, *Chem. Rev.*, **2001**, *101*, 1629. d) D. Braga, F. Grepioni, G. R. Desiraju, *Chem. Rev.*, **1998**, *98*, 1375 and references therein.

[2] J. W. Steed, J. L. Atwood, *Supramolecular Chemistry*; Wiley: New York, 2000.

[3] K. R. Dunbar, R. A. Heintz, *Prog. Inorg. Chem.*, **1997**, *45*, 283 and references therein.

[4] a) P. Rigo, A. Turco, Coord. *Chem. Rev.*, **1974**, *13*, 133; b)W. P. Griffith, *Cood. Chem. Rev.*, **1975**, *17*, 177; c)L. H. Jones, B. I. Swanson, *Acc. Chem. Rev.*, **1976**, *9*, 128; d)A. M. Golub, H. K. H. Kohler, V. V. Skopenko, in *Chemistry of Pseudohalides*, Monogragh21, R. J. H. Clark, Ed., Elsevier, New York, 1986, pp. 77-185; e)A. G. Sharp, in *Comprehensive Coordination Chemistry*, G. Wilkinson, R. D. Gillard, J. A. McCleverty, Eds., Pergamon, New York, Vol. 2, 1987, pp.7-14; f)W. P. Fehlhammer, M. Fritz, *Chem. Rev.*, **1993**, *93*, 1243.

[5] K. A. Hofmann, F. A. Kuspert, *Z. Anorg. Allg. Chem.*, **1897**, *15*, 204.

[6] T. Iwamoto, in *Comprehensive Supramolecular Chemistry*; J. L. Atwood, J. M. Lehn Eds., Pergamon, New York, 1996; Vol. 7, pp. 643-690 and references therein.

[7] a) H. M. Powell, J. H. Rayner, *Nature (London)*, **1949**, *163*, 566; b) J. H. Rayner, H. M. Powell, *J. Chem. Soc.*, **1952**, 319.

[8] T. Iwamoto, in *Inclusion Compounds,* J. L. Atwood, J. E. D. Davies, D. D. Macnicol, Eds., Oxford University Press, Oxford, 1991, Vol. 5, pp. 177-212 and references therein.

[9] a) S. S. Kaye, J. R. Long, *J. Am. Chem. Soc.*, **2005**, *127*, 6506. b) K. W. Chapman, P. D. Southon, C. L. Weeks, C. J. Kepert, *Chem. Comm.*, **2005**, 3322.

[10] K. Nakamoto, *Infrared and Raman spectra of inorganic and coordination compounds*; 5th ed.; John Wiley & Sons, New York; Chichester, England, 1997.

[11] A. R. West, *Basic Solid State Chemistry*; 2nd ed.; Wiley: New York, 1999.

[12] B. F. Hoskins, R. Robson, *J. Am. Chem. Soc.*, **1990**, *112*, 1546.

[13] R.D.Curtis, C. I. Ratcliffe, J. A.Ripmeester, *J. Chem. Soc., Chem. Commun.*, **1992**, 1800.

[14] J. Pickardt, B. Staub, *Z. Naturforsch., B*, **1995**, *50*, 1517.

[15] A. G. Sharpe, The Chemistry of Cyano Complexes of the Transition Metals, Academic Press, New York, 1976.

[16] H. Pearson, *Acta. Chem. Scand.,* **1971**, *25*, 543

[17] E. Colacio, R. Kivekas, F. Lloret, M. Sundberg, J. Suarez-Varela, M. Bardaji, A. Laguna, *Inorg. Chem.*, **2002**, *41*, 5141.

[18] A. Yuan, J. Zou, B. Li, Z. Zha, C. Duan, Y. Liu, Z. Xu and S. Keizer, *Chem. Comm.,* **2000**, 1297.

[19] H. L. Hermann, G. Boche, P. Schwerdtfeger, *Chem. Eur. J.,* **2001**, *7*, 5333.

[20] F. B. Stocker, T. P. Staeva, C. M. Rienstra, D. Britton, I*norg. Chem.,* **1999**, *38*, 984.

[21] L. Ouyang, P. M. Aguiar, R. J. Batchelor, S. Kroeker, D. B. Leznoff, *Chem. Comm.*, **2006**, 744-746.

[22] H. Zhang, J. Cai, X.-L. Feng, B.-H. Ye, X.-Y. Li, L.-N. Ji, *J. Chem. Soc., Dalton Trans.*, **2000**, 1687; N. Mondal, M. K. Saha, B. Bag, S. Mitra, V. Gramlich, J. Ribas ,M. S. El Fallah, *J. Chem. Soc., Dalton Trans.*, **2000**, 1601; T. K. Maji, P. S. Mukherjee, G. Mostafa, E. Zangrando, N. R. Chaudhuri, *Chem. Comm.*, **2001**, 1368; I. Escorihuela, L. R. Falvello,M. Tomas, *Inorg. Chem.*, **2001**, *40*, 636.

[23] M. Ohba, H. Okawa, *Coord. Chem. Rev.*, **2000**, *198,* 313.

[24] K. Wasielewski, R. Mattes, *Z. Naturforsch.* **1992**, *47B*, 1795.

[25] a) J. M. Zheng, S. R. Batten, M. Du, *Inorg. Chem.*, **2005**, *44*, 3371; b) R. J. Williams, D. T. Cromer, A. C. Larson, *Acta Crystallogr., Sect. B* **1971**, *27*, 1701.

[26] E. Moles, R. Izaguirre, *Anal. Fis. Quim. (Madrid),* **1921**, *19*, 33.

[27] T. Pretsch, H. Hartl, *Z. Anorg. Allg. Chem.*, **2004**, *630*, 1581.

[28] a) D. J. Chesnut, A. Kusnetzow, R. Birge, J. Zubieta, *J. Chem. Soc., Dalton Trans.*, **2001**, 2581 and references therein; b) E. Colacio, J. M. Dominguez-Vera, F. Lloret, J. M. M. Sanchez, R. Kivekas, A. Rodriguez, R. Sillanpaa, *Inorg. Chem.*, **2003**, *42*, 4210.

[29] a) T. Kitazawa, S. Nishikiori, R. Kuroda, T. Iwamoto, *J. Chem. Soc., Dalton Trans.*, **1994**, 1029; b) T. Kitazawa, S. Nishikiori, A. Yamagishi, R. Kuroda, T. Iwamoto, *J. Chem. Soc., Chem. Comm.,* **1992**, 413; c)T. Kitazawa, S. Nishikiori, R. Kuroda, T. Iwamoto, *Chem. Lett.,* **1988**, 1729.

[30] J. Cernak, J. Chomic, P. Domoano, O. Ori, A. D. Andreetti, *Acta Crystallogr., Sect. C*, **1990**, *46*, 2103.

[31] I. Muga, J. M. Gutierrez-Zorrilla, P. Vitoria, P. Roman, L. Lezama, J. I. Beitia, *Eur. J. Inorg. Chem.*, **2004**, 1886.

[32] O. Kahn, Molecular Magnetism, VCH: Weinheim, Germany, 1993.

[33] a) T. M. L. Wigley, R. Richels, J. A. Edmonds, *Nature* **1996**, *379*, 240; b) W. C. Sailor, D. Bodansky, C. Braun, S. Fetter, B. van der Zwaan, *Science,* **2000**, *288*, 1177 and references therein.

[34] "Grand challenge for basic and applied research on hydrogen storage: statement of objectives" available at www.eere.energy.gov/hydrogenand-fuelcells/docs/gc_h2_storage.doc.

[35] W. P. Teagan, M. Rona, presentation for the *Hydrogen Storage Materials workshop*, United States Department of Energy, Argonne, IL, August 14-15, **2002**.

[36] G. Sandrock, *J. Alloys Compd.*, **1999**, *293-295*, 877.

[37] L. Schlapbach, *MRS Bull.* **2002**, *27*, 675.

[38] a) P. Benard, R. Chahine, *Langmir* **2001**, *17*, 1950; b) G. G. Tibbetts, G. P. Meisner, C. H. Olk, *Carbon*, **2001**, *39*, 2291.

[39] A. Zuttel, P. Sudan, P. Mauron, T. Kiyobayashi, C. Emmenegger, *L. Schlapbach, Int. J. Hydrogen Energy,* **2002**, *27*, 203.

[40] a) M. J. Zaworotko, *Chem. Soc. Rev.,* **1994**, 283; b) J. S. Moore, S. Lee, *Chem. Ind.,* **1994**, 556; c) M. D. Ward, *Nature,* **1995**, *374*, 764; d) C. L. Bowes, G. A. Ozin, *Adv. Mater.,* **1996**, *8*, 13 and references therein.

[41] a) G. Ferey, M. Latroche, C. Serre, F. Millange, T. Loiseau, A. PercheronGuegan, *Chem. Comm.*, **2003**, 2976; b) J. L. C. Rowsell, O. M. Yaghi, *Angew. Chem. Int. Ed.* **2005**, *44*, 4670 and references therein.

[42] H. K. Chae, D. Y. Siberio-Perez, J. Kim, Y. Go, M. Eddaoudi, A. J. Matzger, M. O'Keeffe and O. M. Yaghi, *Nature*, **2004**, *427*, 523.

[43] K. S. W. Sing, D. H. Everett, R. A. W. Haul, L. Moscou, R. A. Pirrotti, J. Rouquerol, T. Siemieniewska, *Pure Appl. Chem.,* **1985**, *57*, 603.

[44] L. Pan, M. Sander, X. Y. Huang, J. Li, M. Smith, E.Brittner, B. Bockrath, J. K. Johnson, *J. Am. Chem. Soc.*, **2004**, *126*, 1308.

[45] B. Chen, N. W. Ockwig, A. R. Millward, D. S. Contreras, O. M. Yaghi, *Angew. Chem.,* **2005**, *117*, 4823; *Angew. Chem. Int. Ed.,* **2005**, *44*, 4745.

[46] J. Lefebvre, R. J. Batchelor, D. B. Leznoff, *J. Am. Chem. Soc.,* **2004,** *126,* 16117.

[47] S. J. Gregg, K. S. W. Sing, *Adsorption, Surface Area and Porosity*, 2nd Ed., New York, 1982 and references there in.

[48] S. Ross, J. P. Olivier, *On Physical Adsorption*, Interscience Publishers, New York, 1964.

[49] a) M. Kirk, M. Jaroniec, *Chem. Mater.*, **2001**, *13*, 3169; b) F. Rouquerol, J. Rouquerol, K. Sing, *Adsorption by powders and Porous Solids*, Academic Press, San Diago, **1999**; c) J. P. Oliver, *Fundamentals of Adsorption*, Kluwer, Boston, **1996**.

[50] S. Brunauer, *The Adsorption of Gases and Vapors. Vol. I. Physical Adsorption*, Princeton University Press, Princeton, N.J., 1943.

[51] K. S. W. Sing, D. H. Everett, R. A. W. Haul, L. Moscou, R. A. Pierotti, J. Rouquerol, T. Siemieniewska, *Pure Appl. Chem.*, **1985**, *57*, 603.

[52] I. Langmuir, *J. Am. Chem. Soc.*, **1916**, *38*, 2221.

[53] R. Sips, *J Chem. Phys.*, **1948**, *16*, 490.

[54] S. Brunauer, P. H. Emmett, E. Teller, *J. Am. Chem. Soc.*, **1938**, *60*, 309.

[55] L. Jelinek, E. sz. Kovats, *Langmuir*, **1994**, *10*, 4225.

[56] A. K. Brimah, E. Siebel, R. D. Fischer, N. A. Davies, D. C. Apperley, R. K. Harris, *J. Organomet. Chem.*, 1994, *475*, 85.

[57] L. S. Erre; G. Micera, F. Cariati, G. Ciani, A. Sironi, H. Kozlowski, J. Baranowski, *J. Chem. Soc., Dalton Trans.* **1988**, 363.

[58] J. L. C. Rowsell, A. R. Millward, K. S. Park, O. M. Yaghi, *J. Am. Chem. Soc.*, **2004**, *126*, 5666.

[59] a) J. F. Keggin, F. D. Miles, *Nature*, **1936**, *137*, 577. b) H. J. Buser, A. Ludi, W. Peter, D. Schwarzenbach, *J. Chem. Soc., Chem. Commun.* **1972**, 1299; H. J. Buser, D. Schwarzenbach, W. Peter, A. Ludi, *Inorg. Chem.*, **1977**, *16*, 2704; F. Herren, P. Fischer, A. Ludi, W. Halg, *Inorg. Chem.*, **1980**, *19*, 956.

[60] E. J. Gabe, P. S. White, G. D. Enright, *DIFRAC A Fortran 77 Control Routine for 4-Circle Diffractometers*; N. R. C.: Ottawa, 1995.

[61] E. J. Gabe, Y. LePage, J. P. Charland, F. L. Lee, P. S. White, *J. Appl. Cryst.*, **1989**, *22*, 384.

[62] D. J. Watkin, C. K. Prout, J. R. Carruthers, P. W. Betteridge, R. I. Cooper, *CRYSTALS Issue 11, Chemical Crystallography Laboratory*; University of Oxford: Oxford, 1999.

[63] a) R. Taylor, C. F. Macrae, *Acta Crystallogr.* B57, **2001**, 815-827. b) I. J. Bruno, J. C. Cole, P. R. Edgington, M. K. Kessler, C. F. Macrae, P. McCabe, J. Pearson, R. Taylor, *Acta Crystallogr.* B58, **2002**, 389-397. c) C. F. Macrae, P. R. Edgington, P. McCabe, E. Pidcock, G. P. Shields, R. Taylor, M. Towler, J. van de Streek, *J. Appl. Cryst.*, **2006**, *39*, 453-457.